OPEN ACCESS

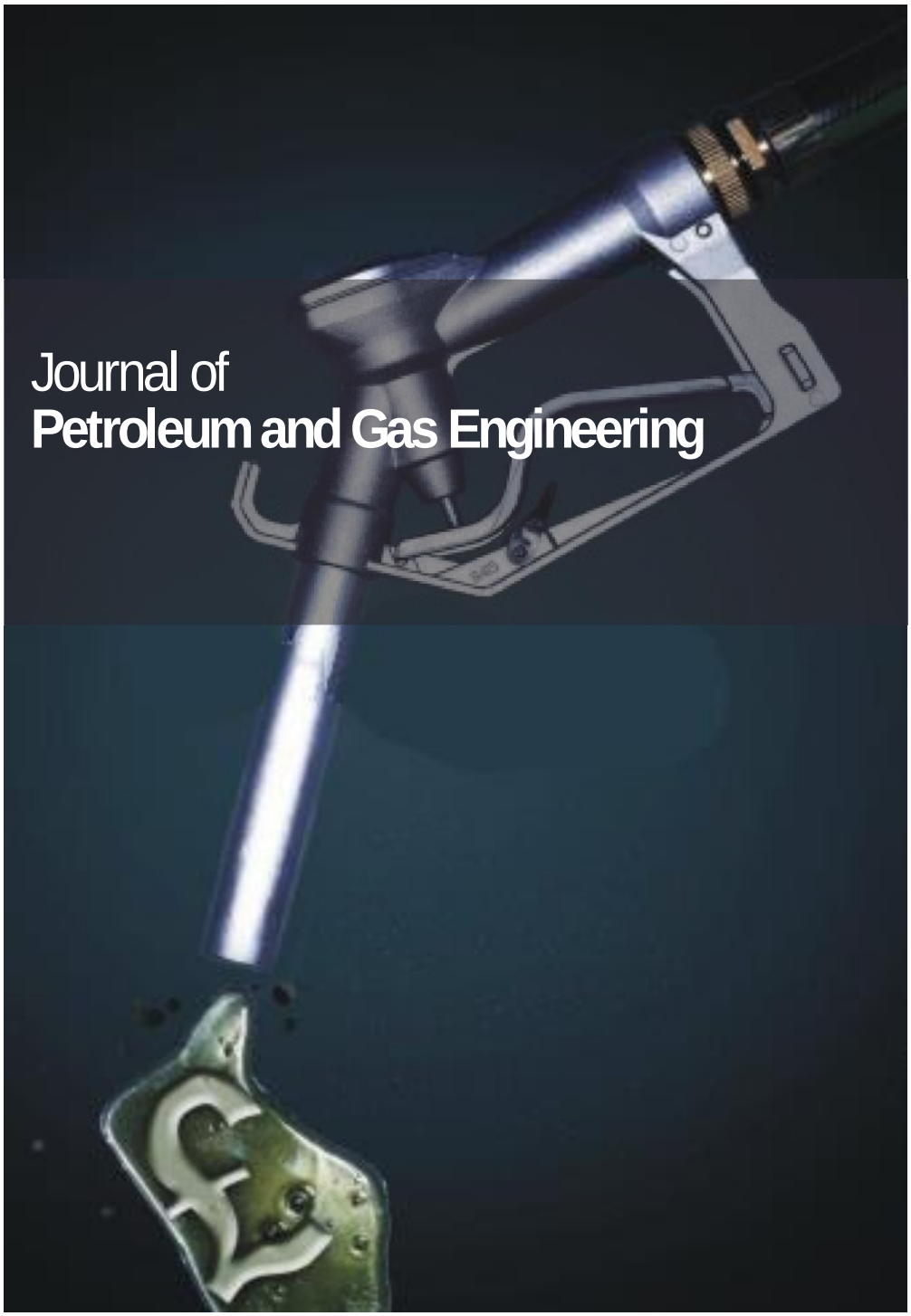

Journal of Petroleum and Gas Engineering

July-September 2019
ISSN 2141-2677
DOI: 10.5897/JPGE
www.academicjournals.org

ACADEMIC JOURNALS
expand your knowledge

About JPGE

Journal of Petroleum and Gas Engineering (JPGE) is a peer reviewed journal. The journal is published per article and covers all areas of the subject such as: Petroleum geology, Reservoir simulation, Enhanced oil recovery, subsurface analysis and Drilling technology.

Open Access Policy

Open Access is a publication model that enables the dissemination of research articles to the global community without restriction through the internet. All articles published under open access can be accessed by anyone with internet connection.

The Journal of Petroleum and Gas Engineering is an Open Access journal. Abstracts and full texts of all articles published in this journal are freely accessible to everyone immediately after publication without any form of restriction.

Article License

Memberships and Standards

Academic Journals strongly supports the Open Access initiative. Abstracts and full texts of all articles published by Academic Journals are freely accessible to everyone immediately after publication.

All articles published by Academic Journals are licensed under the Creative Commons Attribution 4.0 International License (CC BY 4.0). This permits anyone to copy, redistribute, remix, transmit and adapt the work provided the original work and source is appropriately cited.

Crossref is an association of scholarly publishers that developed Digital Object Identification (DOI) system for the unique identification published materials. Academic Journals is a member of Crossref and uses the DOI system. All articles published by Academic Journals are issued DOI.

Similarity Check powered by iThenticate is an initiative started by CrossRef to help its members actively engage in efforts to prevent scholarly and professional plagiarism. Academic Journals is a member of Similarity Check.

CrossRef Cited-by Linking (formerly Forward Linking) is a service that allows you to discover how your publications are being cited and to incorporate that information into your online publication platform. Academic Journals is a member of CrossRef Cited-by.

Academic Journals is a member of the International Digital Publishing Forum (IDPF). The IDPF is the global trade and standards organization dedicated to the development and promotion of electronic publishing and content consumption.

COUNTER (Counting Online Usage of Networked Electronic Resources) is an international initiative serving librarians, publishers and intermediaries by setting standards that facilitate the recording and reporting of online usage statistics in a consistent, credible and compatible way. Academic Journals is a member of COUNTER

Portico is a digital preservation service provided by ITHAKA, a not-for-profit organization with a mission to help the academic community use digital technologies to preserve the scholarly record and to advance research and teaching in sustainable ways.

Academic Journals is committed to the long-term preservation of its content and uses Portico

Academic Journals provides an OAI-PMH(Open Archives Initiatives Protocol for Metadata Harvesting) interface for metadata harvesting.

Contact

Editorial Office: jpge@academicjournals.org

Help Desk: helpdesk@academicjournals.org

Website: http://www.academicjournals.org/journal/ JPGE

Submit manuscript online http://ms.academicjournals.org

Academic Journals

73023 Victoria Island, Lagos, Nigeria

ICEA Building, 17th Floor, Kenyatta Avenue, Nairobi, Kenya

Editors

Table of Content

Vol. 10(4), pp. 49-54, July –September 2019
DOI: 10.5897/JPGE2019.0319
Article Number: 9394BAA61661
ISSN: 2I41-2677

http://www.academicjournals.org/JPGE

ACADEMIC JOURNALS

Journal of Petroleum and Gas Engineering

Full Length Research Paper

Probabilistic approach for shale volume estimation in Bornu Basin of Nigeria

Stephen Adjei[1*], Aggrey N. Wilberforce[2], Daniel Opoku[1] and Isah Mohammed[1]

[1]Petroleum Engineering Department, College of Petroleum Engineering, King Fahd University of Petroleum and Minerals, Saudi Arabia.
[2]Petroleum Engineering Department, College of Engineering, Kwame Nkrumah University of Science and Technology, Ghana.

Received 22 May, 2019; Accepted 24 July, 2019

The gamma ray log has over the years provided the conventional means for shale volume (Vsh) estimation. Knowledge of Vsh is used in the prediction of petrophysical parameters like effective porosity and water saturation, which are the input parameters for the calculation of oil in place. Currently, many studies have been conducted on the Bornu Basin of Nigeria, to access its hydrocarbon potential. Unfortunately, the practice of using best gamma ray log value for the computation of gamma ray index, I_{GR}, and subsequently Vsh estimation incorporates huge uncertainty in the estimated volumes. Uncertainty is best captured when estimates are represented in a possible range rather than single value measurements. To the best of our knowledge, this is the first time shale volume has been estimated from the gamma ray log using sampling techniques. The gamma ray log data of the two upper shaly intervals of the NGAMMAEAST_1 well, which penetrates the Gombe formation of the basin, were utilized for this study. The gamma ray log response of the zone of interest is the uncertain parameter in Vsh estimation. A histogram plot of the uncertain log data was used to assume the probability distribution of the data. In the MATLAB platform, Standard Monte Carlo (MC) and Latin Hypercube sampling techniques were used to model the uncertain log response using random numbers. Possible input log data generated from the distribution of the uncertain log data were used in the linear and non-linear models for shale volume estimation to run a series of simulations to determine the possible range of estimates with their probabilities. The Latin hypercube method has shown to be a quick and accurate alternative method to the standard MC method. The approach presented here sets a guideline for the implementation of a probabilistic approach for the volume of shale estimation.

Key words: Shale volume, Monte Carlo, Latin hypercube, sampling techniques, gamma ray log.

INTRODUCTION

The government of Nigeria has currently reopened its interest in exploring the hydrocarbon potential of the Bornu basin. This basin forms a part of the huge Chad basin. Earlier exploration activities were unsuccessful due to non-commercial discoveries. However, the discovery of commercial quantities of hydrocarbons in other areas of the basin lying in countries like Chad, Niger and the Central African Republic has revived the

*Corresponding author. E-mail: adjeistephen89@gmail.com.

the government's commitment to exploring the basin. The stratigraphy of the basin is made up of different formations (Bima, Fika, Gongila, Kerri-Kerri, Gongila, Yolde, Chad) composed of sandstone, shale, siltstone, and limestone (Adekoya et al., 2014). Detail description of the basin can be found in works published by (Ali and Orazulike, 2011; Hamza and Hamidu, 2012). Over the past few years, there have been intensive studies on various areas of the basin. Ola et al. (2017) evaluated the potential of the source rock at the south-western section of the basin using rock samples from three different wells. The authors identified the area to be predominantly gas-prone with oil shows in one of the wells. Similar results were obtained by Obaje et al. (2004) who studied the quality of source rock using samples from four different wells. Obaje et al. (2004) in their work, identified over 80% of samples from the wells to contain a total organic content above 0.5 wt.%. Mohammed and Tela (2012) used the particle size and the depositional setting of sediments to determine the hydrocarbon potential of the basin. Sanusi and Mickus (2014) used geophysical data to study the structural configuration of the basin while Adepelumi et al. (2011) did a petrophysical analysis of the Gombe formation.

Shale volume (Vsh) estimation is a significant step in formation evaluation. Vsh is an expression of the fraction of the total amount of clay and other particles such as silt to the total rock volume (Szabó, 2011). The estimated Vsh are used in the prediction of petrophysical parameters like effective porosity and water saturation from which the hydrocarbon in place can be estimated (Airuwaili and Alwaheed, 2004). Knowledge of the reservoir shaliness guides in the evaluation of the rock's quality (Ali and Orazulike 2011). Though Vsh estimation can be done using data from the density-neutron log, spontaneous log, the resistivity log, and other methods, the gamma ray log has served as the conventional means of computing the shale volume. Equation 1 is the linear model for Vsh estimation using the gamma ray log. The model estimates the gamma ray index, IGR, of the shaly interval and assumes it to be the Vsh of the interval (Hamada, 1996; Adam and Bashar, 2017).

$$I_{GR} = Vsh = \frac{G - G_{cleansand}}{G_{shale} - G_{cleansand}} \quad (1)$$

where I_{GR} is a gamma ray index, Vsh is the volume of shale, G is gamma ray reading in the zone of interest, $G_{cleansand}$ is gamma response in clean sand and G_{shale} is the gamma ray response in shaly or clay bed.

Nonlinear model for Vsh estimation

The linear model approach assumes the formation to contain only shale and clay minerals. This assumption tends to overestimate the shale volume in zones containing other radioactive minerals. A number of non-linear models defined for certain formation ages and geographic areas have been formulated to mitigate the uncertainties associated with the linear model (Worthington, 2008; David et al., 2015). The Larinov models for tertiary and older rocks and the Steiber and Clavier models are given in Equations 2 to 5.

Larinov (1969) for tertiary rocks

$$V_{sh} = 0.083(2^{3.7 I_{GR}} - 1) \quad (2)$$

Larinov (1969) for older rocks

$$V_{sh} = 0.33(2^{2 I_{GR}} - 1) \quad (3)$$

Steiber (1970)

$$V_{sh} = \left(\frac{I_{GR}}{3 - 2 I_{GR}} \right) \quad (4)$$

Clavier (1971)

$$V_{sh} = 1.7 - \left[\left(3.38 - \left(I_{GR} + 0.7 \right)^2 \right) \right]^{\frac{1}{2}} \quad (5)$$

It can be seen that these non-linear models rely on the computed I_{GR} from the linear model as input for their prediction. However, the common approach of using best gamma ray log value of the zone of interest for I_{GR} computation incorporates huge uncertainty in the estimated I_{GR}, which is, propagated through these non-linear models and hence undermining their accuracy. The conventional approach for Vsh estimation used in the Bornu basin and the petroleum industry at large has been deterministic and performed under huge uncertainty. This has resulted in huge discrepancies in published works. This paper seeks to illustrate the role of sampling techniques in mitigating the uncertainty in the input parameters and to recommend their application in the volume of shale estimation in the Bornu basin and the petroleum industry at large.

Standard Monte Carlo and Latin hypercube techniques

The Standard Monte Carlo (MC) and Latin Hypercube Simulation (LHS) are methods that provide a stochastic approach for uncertainty evaluation. In these techniques, the uncertain parameter is modeled using random numbers. In this way, possible input values obtained are used in a series of simulations to determine a range of estimates with their probabilities. One main advantage of the MC method is that it is independent of the number of input random samples (Alkhatib and King, 2013).

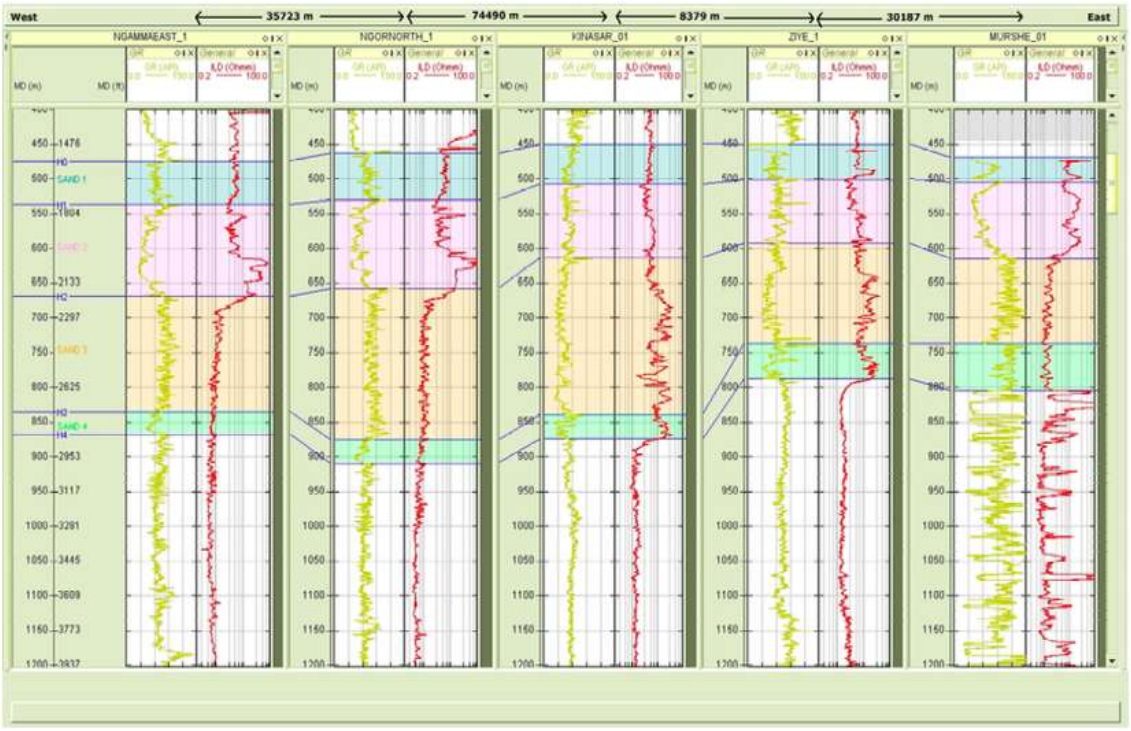

Figure 1. Log data of NGAMMA_1 well.

Table 1. NGAMMAEAST_1 Well Log Data.

Sand Unit	Thickness (m)	K (md)
Sand 1	62.30	9986.74
Sand 2	131.63	18948.68

K = Permeability.
Source: Adepelumi et al. (2011).

However, it requires large computational times to achieve accuracy due to its low convergence rate, with a convergence rate of $1/\sqrt{N}$, where N is the number of paths or realizations (Xiu, 2007). Also, due to its randomness, it sometimes results in clustering. Unlike the Standard MC, the LHS is a controlled randomization technique. The distribution of the input data is partitioned into even intervals of equal probability. A sample is selected from each interval and used in repeated simulations. The process requires less iteration to achieve accuracy (Nathanail and Rosenbaum, 1991).

METHODOLOGY

Data

This illustration was done using the NGAMMAEAST_1 well, which penetrates the Gombe formation of the Bornu basin. The log data, obtained from Adepelumi et al. (2011), was made available by the Nigerian National Petroleum Corporation. The log is given in Figure 1. The properties of the zone of interest for this study are reported in Table 1.

Procedure

Uncertainty evaluation using the sampling techniques for I_{GR} and Vsh computation was illustrated using only the top two shaly intervals of the well; Sand 1 (depth of 475-540 m) and Sand 2 (depth of 540-670 m). From Equation 1, the gamma ray response in the clean sand and that in the shaly interval are assumed constant; 30 and 148 American Petroleum Institute (API) units respectively. The gamma ray log value in the zone of interest is the uncertain input parameter in the volume of shale estimation models. The first step was to determine the distribution of the log data in the zone of interest. For Sand 1, the thickness was divided into 10 equal intervals and three log values were picked from each interval. A histogram of the sampled data was then generated to determine the distribution of the log values. The procedure was repeated for Sand 2 but with 20 divisions. The distributions of the input log values for both sand intervals were assumed to follow the normal distribution, (Figure 2). The probability and cumulative density functions of the

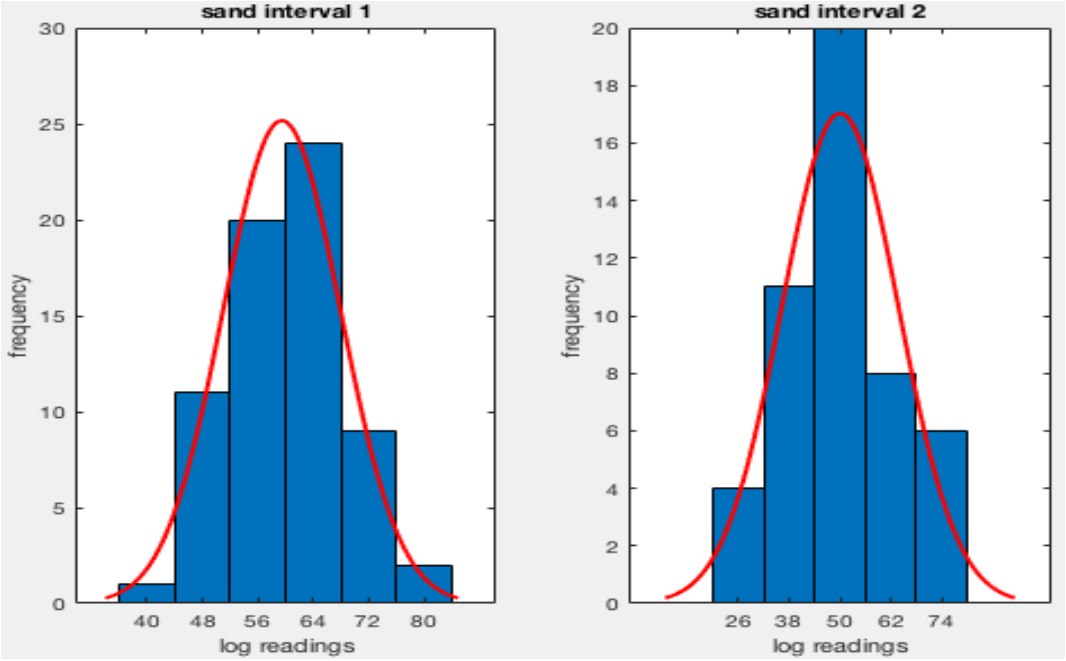

Figure 2. Distribution of Input Data for Sand 1 and 2.

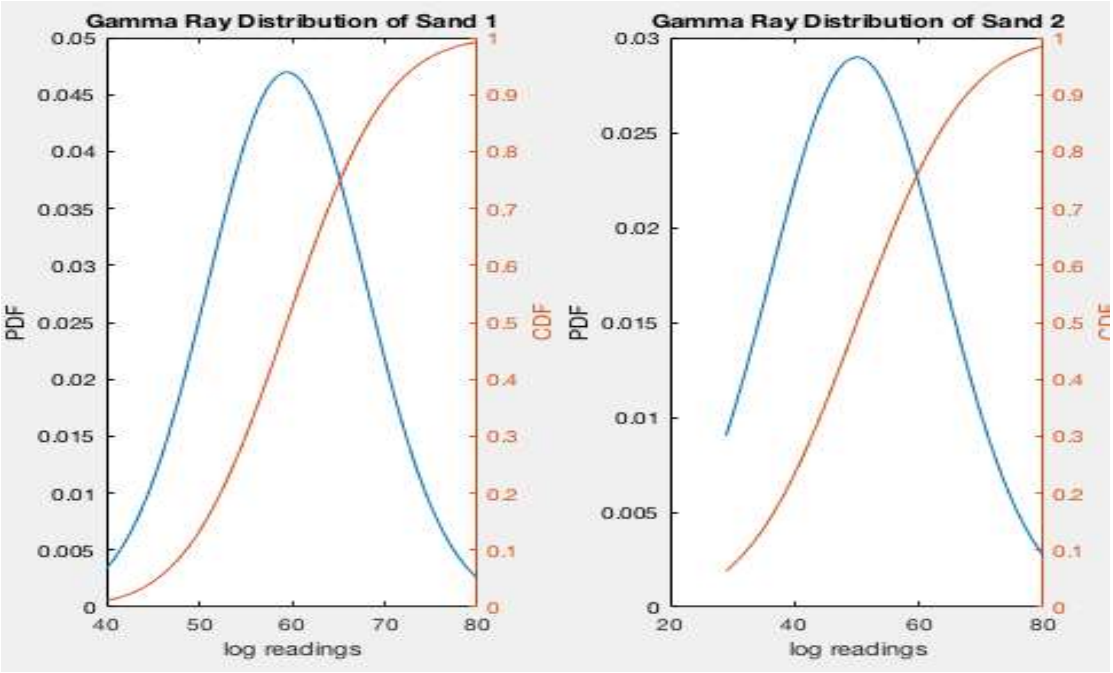

Figure 3. Density and cumulative density function plots of input data.

input data are plotted in Figure 3. To implement probabilistic techniques, the log data is modeled as random variables. Monte Carlo (MC) and Latin hypercube sampling methods were used to sample from the cumulative distribution of the uncertain input log data. In the case of the LHS technique, the cumulative distribution function of the input log data was divided into 5 intervals of equal probability from which a sample was taken from each interval. These sampled data were then used in the linear model to determine the shale volume of the intervals. The P10, P50, and P90 of the estimates were then computed. The generation of the cumulative distribution and probability density functions of the log data, sampling and simulation were done using the MATLAB

Table 2. Monte Carlo simulation for sand 1.

Percentiles	Vsh				
	Linear (%)	Larinov tertiary (%)	Larinov old (%)	Steiber (%)	Clavier (%)
P10	16.2	4.0	7.6	6.0	7.7
P50	25.6	7.5	12.5	10.0	12.6
P90	34.9	11.7	18.3	14.8	18.6

Table 3. Monte Carlo simulation for sand 2.

Percentiles	Vsh				
	Linear (%)	Larinov tertiary (%)	Larinov Old (%)	Steiber (%)	Clavier (%)
P10	5.0	1.5	2.7	2.2	2.7
P50	19.2	5.6	9.6	7.7	9.7
P90	35.0	12.5	19.3	15.7	19.6

Table 4. Latin hypercube simulation for sand 1.

Percentile	Vsh				
	Linear (%)	Larinov tertiary (%)	Larinov old (%)	Steiber (%)	Clavier (%)
P10	15.7	4.1	7.3	5.9	7.4
P50	25.0	7.5	12.4	10.0	12.6
P90	34.2	11.7	18.2	14.7	18.5

Table 5. Latin hypercube simulation for sand 2.

Percentile	Vsh				
	Linear (%)	Larinov tertiary (%)	Larinov old (%)	Steiber (%)	Clavier (%)
P10	1.3	0.3	0.5	0.4	0.5
P50	19.0	5.2	9.0	7.2	9.0
P90	36.7	13.0	20.0	16.2	20.0

language.

RESULTS AND DISCUSSION

Determination of Vsh requires the estimation of I_{GR}. For a given I_{GR}, the Vsh is then estimated using different models. The conventional deterministic approach for shale volume estimation is based on user experience, resulting in huge uncertainties. Sampling techniques provide a means of minimizing the error associated with the estimation of the I_{GR} and hence Vsh. Two zones of the Gombe Formation in the Bornu Basin, penetrated by the NGAMMAEAST_1 well have been used to illustrate the significance of sampling techniques in predicting the shaliness of a formation. The performance of two sampling techniques has been studied. The Monte Carlo sampling is based on random sampling from the distribution of the uncertain input data. The MC method requires large iterations to achieve accuracy due to its slow convergence rate. The results in this paper are based on 2000 samples. Over the years, there have been various improvements to the MC technique. LHS is a new technique that tends to approach MC accuracy using fewer data points. Unlike in the deterministic method, which yields single value measurements, probabilistic techniques yield a wide range of estimates with their associated probabilities. These values represent optimistic and pessimistic estimates, which are critical in decision making. The P10, P50 and P90 values for the linear and non-linear models computed from the realizations of the Monte Carlo simulation have been reported in Tables 2 and 3 for Sand 1 and 2 respectively. Similarly, the results from the LHS are reported in Tables 4 and 5 for Sand 1 and 2 respectively. It is observed that

the computed P10, P50 and P90 values are similar for both sampling techniques for Sand 1, though in the Latin hypercube method fewer data points were used. The LHS, therefore, provides an efficient alternative to the conventional MC method. For Sand 2, the computed P50 and P90 using both techniques yielded similar results. However, there were huge variations in the P10 values for all models. Monte Carlo results are reliable in such situations as it uses more data points.

Comparing the results of this study to those in literature for the same well and sand intervals, it was observed that a number of authors have deterministically computed the I_{GR} and subsequently Vsh. In highly heterogeneous formations, the errors associated with this approach are substantial. Results from this study have shown that the linear model for the computation of shale volume, which assumes the Vsh to be linearly proportional to the I_{GR}, overestimates the shale volume. For a given I_{GR}, it is observed that the Larinov model for older rocks and the Clavier model give similar results while the Larinov model for tertiary rocks yields the least estimates.

Conclusion

This work outlines the approach in using sampling techniques in predicting the gamma ray index and subsequently the shaliness of sand intervals in the Bornu Basin of Nigeria. The following conclusions were made:

(i) The conventional deterministic approach in shale volume estimation results in huge errors propagated through the input parameters.
(ii) The probabilistic approach mitigates the uncertainty in the estimate by providing a possible range of estimates with their associated probabilities unlike the single value estimates of the deterministic approach.
(iii) The Latin hypercube technique is a quick approach that provides an efficient means of sampling and uncertainty analysis using fewer data points.
(iv) The linear model overestimates the shale volume.

CONFLICT OF INTERESTS

The authors have not declared any conflict of interests.

REFERENCES

Adam E, Mohammed B (2017). Correct Shale Volume Estimation and Clay Typing Identification in Shaly Sand Reservoirs: Case Study of Zarga Formation , Keyi Oil Field 18(1):22-33.

Adekoya JA, Ola PS, Olabode SO (2014). Possible Bornu Basin Hydrocarbon Habitat- A Review. International Journal of Geoscience 5:983-996.

Adepelumi AA, Alao OA, Kutemi TF (2011). Reservoir Characterization and Evaluation of Depositional Trend of the Gombe Sandstone, Southern Chad Basin Nigeria. Journal of Petroleum and Gas Engineering 2(6):118-131.

Airuwaili SB, Alwaheed HH (2004). Petrophysical Models and Techniques for Shaly-Sand Formation Evaluation. Society of Petroleum Engineers, 11th ADIPEC: Abu Dhabi International Petroleum Exhibition and Conference pp. 261-272.

Ali S, Orazulike DM (2011). Estimation of the Petrophysical Parameters of Sediments from Chad Basin Using Well Logs. Global Journal of Geological Sciences 9(2).

Alkhatib A, King P (2013). Uncertainty Quantification of a Chemically Enhanced Oil Recovery Process : Applying the Probabilistic Collocation Method to a Surfactant-Polymer. SPE Middle East Oil and Gas Show and Conference, Manama, Bahrain.

David SO, Rodolfo SB, Jonathan SO, Pasquel O, Arteaga D (2015). A universal Equation to Calculate Shale Volume for Shaly-sands and Carbonate Reservoirs. In SPE Latin American and Caribbean Petroleum Engineering Conference, Quito, Ecuador, 18-20 Novermber. Society of Petroleum Engineers.

Hamada GM (1996). An Integrated Approach to Determine Shale Volume and Hydrocarbon Potential in Shaly Sand. Presented at SCA International Symposium pp. 2093-107.

Hamza H, Hamidu I (2012). Hydrocarbon Resource Potential of the Bornu Basin Northeastern Nigerian. Global Journal of Geological Sciences 10(1):71-84.

Mohammed YB, Tela B (2012). Assessment of Tertiary Sediments Of Bornu Basin for Possible Hydrocarbon Reservoir 1(4):251-257.

Nathanail CP, Rosenbaum MS (1991). Probabilistic slope stability assessment using Latin Hypercube Sampling." 7th ISRM Congress. International Society for Rock Mechanics and Rock Engineering.

Obaje NG, Wehner H, Hamza H, Scheeder G (2004). New Geochemical Data from the Nigerian Sector of the Chad Basin: Implications on Hydrocarbon Prospectivity. Journal of African Earth Sciences 38(5):477-487.

Ola PS, Adekoya JA, Olabode OS (2017). Source Rock Evaluation in the Lake Chad Area of the Bornu Basin, Nigeria. Journal of Petroleum and Environmental Biotechnology 8:346. doi: 10.4172/2157-7463.1000346

Sanusi A, Mickus K (2014). Gravity and Magnetic Analysis of the Bornu Basin, Northeast Nigeria. Geological Society of America Annual Meeting in Vancouver, Canada.19-22 October

Szabó NP (2011). Shale volume estimation based on the factor analysis of well-logging data. Acta Geophysica 59(5):935.

Worthington PF (2008). Quality-Assured Evaluation of Effective Porosity Using Fit-for-Purpose Estimates of Shale Volume Fraction. 49th Annual Logging Symposium, Texas, USA, 25-28 May.Society of Petrophysics and Well-Log Analyssts

Xiu D (2007). Efficient Collocational Approach for Parametric Uncertainty Analysis.Communications in Computational Physics 2(2):293-309.

Vol. 10(4), pp. 55-64, July-September 2019
DOI: 10.5897/JPGE2019.0306
Article Number: C2693A861743
ISSN: 2I41-2677

http://www.academicjournals.org/JPGE

ACADEMIC JOURNALS

Journal of Petroleum and Gas Engineering

Full Length Research Paper

A dry gas material balance with an infinite aquifer influence: A comparative study between the unsteady state model of van Everdingen-Hurst and analytical model

Isac Inácio Tsamba[1*], Luís Helder Lucas[1] and Pål Skalle[2]

[1]Post Graduation Department, Faculty of Engineering, Universidade Eduardo Mondlane, Mozambique.
[2]Department of Geoscience and Petroleum, Norwegian University of Science and Technology, Norway.

Received 13 February, 2019; Accepted 12 July, 2019

Aquifer water influx is an important natural mechanism for primary recovery. It affects the performance of all types of reservoirs, also natural gas reservoirs. Water influx provides pressure support during reservoir depletion, resulting in slower pressure decline. Consequently, gas reservoirs associated with large aquifers show a flattening, cubic behavior of the p/z vs. G_p curve, which allowed the development of the present analytical model. For modelling of water influx into a reservoir, classical models have been developed by many authors. Among the classical models, the unsteady state method of van Everdingen-Hurst was selected to be used in this work, as this is the best suited in terms of solving the diffusivity equation. In order to use the analytical model for comparative purposes, there was a need of calibrating the two unknown parameters, α and β, appearing in the water influx equation. In this work, two workflows were presented for computing water influx in a comparative manner between the unsteady state model of van Everdingen-Hurst and the analytical model. The results showed that the correlation between both models depends on the two unknown parameters, α and β.

Key words: Infinite aquifer, dry gas material balance, cubic cumulative model, water influx.

INTRODUCTION

Most hydrocarbon reservoirs are surrounded by aquifers. Aquifers may in some cases be significantly greater than the gas reservoir, ranging from infinite in size to less than insignificant, with corresponding large to negligible effect on the reservoir performance (Ahmed, 2005).

In reservoirs adjoined by water aquifers, water drive may be the primary production mechanism. In these reservoirs, the production of hydrocarbons causes a pressure drop in the hydrocarbon/water interface. Due to this pressure drop, a pressure differential develops from the surrounding aquifer into the reservoir. Thus, the aquifer reacts by encroaching across the original hydrocarbon-water contact, filling the reservoir pore spaces (Feng et al., 2015).

The invasion of reservoir rock by aquifer water may have a significant impact on reservoir performance.

*Corresponding author. E-mail: isac.tsamba@gmail.com. Tel: +258 826284010/+258 848295401.

Therefore, water influx into hydrocarbon reservoir must be accurately predicted (Shimada, 2009).

In order to calculate the amount of encroaching water influx, mathematical models (Ahmed, 2005) have been developed by different authors, where the following four models stand out: Schilthuis steady state, van Everdingen and Hurst unsteady state, Carter-Tracy unsteady state and Fetkovich pseudosteady state.

Over the years, water influx models have been improved, Agarwal (1967) presented an analytical simplified model for the material balance of gas reservoir experiencing water influx, further improved and presented by Zonoozi and Blansigame (Blansigame and Zonoozi, 2005).

To use Agarwal's model for computing water influx is a challenging task. There is a need of calibrating the unknown parameters α and β for a specific data set. The Agarwal water influx model was further developed in this work, to match the reservoir's historical production and pressure data when incorporated in the material balance for dry gas reservoirs.

The correct identification of reservoir drive mechanism is crucial in arriving at an accurate estimate of in-place volumes (Alattar, 2009). Ignoring the possibility of water influx can lead to a significant over-estimation of gas initially in place (Istiak et al., 2016). For that reason, correct estimation of gas initialy in place (GIIP) is very crucial for reservoir management and decision-making for field development (Istiak et al., 2016).

The general objective of this work is to analyse the correlation between the van Everdingen and Hurst model and cubic cumulative production model hereafter considered as analytical model.

LITERATURE REVIEW

All classical aquifer models are the solutions for diffusivity equation. Accurate estimations of cumulative water influx into gas reservoirs are very crucial for material balance computations in water drive gas reservoirs. In literature, there are several classical aquifer models. Based on that the unsteady state method of van Everdingen-Hurst was selected, among the classical models, to be used in this work, as this is the best suited in terms of solving the diffusivity equation [11],[12].

The analytical model, developed by Agarwal (1967) allows a direct computation of the cumulative water influx.

van Everdingen and Hurst unsteady-state model

The model presented by van Everdingen and Hurst (1949) deals with two types of aquifers: radial and linear. Applying the Laplace transformation, van Everdingen and Hurst solved the diffusivity equation of the reservoir-aquifer system considering as boundary condition a constant terminal pressure (CTP) in the boundary (Alattar, 2009). The final form of the CTP solution is written as:

$$W_e = U\Delta P W_D(t_D) \quad (1)$$

where U is the influx constant of water into the aquifer, in bbl/psia, represented by Equation 2:

$$U = 1.119 f \phi h c_t r_g^2 \quad (2)$$

W_e is the cumulative water influx due to a pressure drop ΔP (psia) imposed at the reservoir radius r_g, at time t = 0, in bbls, $W_D(t_D)$ is a dimensionless water influx function, *f* is the relative encroachment angle ($^o/360^o$), ϕ is the aquifer porosity fraction, c_t is the total aquifer compressibility in $psia^{-1}$, and t_D is the dimensionless time (Marques and Trevisan, 2007).

$$t_D = \frac{2.309 kt}{\phi \mu c_t r_g^2} \quad (3)$$

The dimensionless water influx $W_D(t_D)$ is presented in tabular form or as a set of polynomial expressions giving W_D as a function of t_D for a range of ratios of the aquifer to reservoir radius. In this work, the polynomial approach proposed by Edwardson et al. (1962) is used and found much easier to deal with than the look up tables or charts that may sometimes require interpolations. The proposed polynomial equations proposed by Edwardson essentially approximate the W_D data in three dimensionless time regions (Ahmed, 2005).

(a) For $t_D < 0.01$:

$$W_{eD} = \sqrt{\frac{t_D}{\pi}} \quad (4)$$

(b) For 0.01 < tD < 200:

$$W_{eD} = \frac{\left(1.2838\sqrt{t_D} + 1.19328 t_D + 0.269872 (t_D)^{3/2} + 0.00855294 (t_D)^2\right)}{\left(1 + 0.616599\sqrt{t_D} + 0.041300 8 t_D\right)} \quad (5)$$

(c) For tD > 200

$$W_{eD} = \frac{-4.29881 + 2.02566 t_D}{\ln(t_D)} \quad (6)$$

New $p/Z\text{-}G_p^3$ cubic cumulative production model for the water influx

The cubic cumulative model proposed by Agarwal (1967) is a simplified model for the material balance of gas reservoirs experiencing water influx.

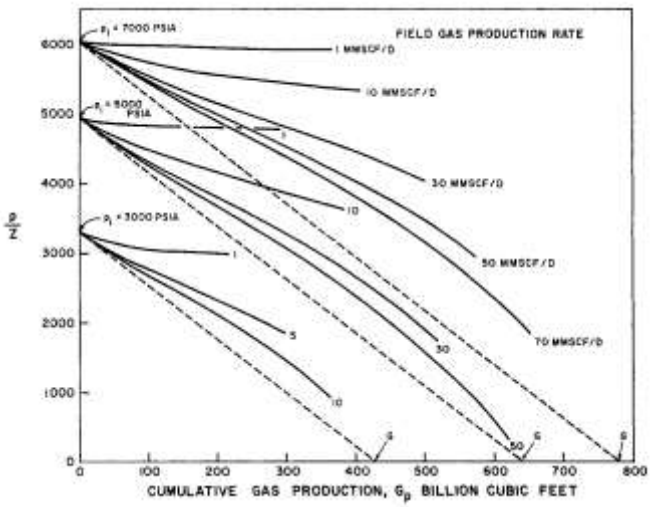

Figure 1. p/z vs Gp Cubic behavior, Agarwal (1967)

This analytical model is based on cubic behavior of the relationship between p/z vs G_p curve as indicated in Figure 1.

Eliminating the abnormal pressure, water production/ injection, and gas injection terms in the general material balance of a dry gas reservoir system and after some mathematical adjustments, it gave the following definition (Blansigame and Zonoozi, 2005):

$$\frac{p}{Z}=\frac{p_i}{Z_i}\frac{1}{\left[1-\frac{W_eB_w}{GB_{gi}}\right]}\left[1-\frac{G_p}{G}\right] \quad (8)$$

To validate the cubic behavior of p/Z vs. G_p performance, we consider the behavior of the "water influx" term:

$$\frac{1}{\left[1-\frac{W_eB_w}{GB_{gi}}\right]} \text{ Versus } \frac{G_p}{G}$$

Thus, the "water influx" term can be written in the form:

$$\frac{1}{\left[1-\frac{W_eB_w}{GB_{gi}}\right]}=\left[1+\alpha\left(\frac{G_p}{G}\right)+\beta\left(\frac{G_p}{G}\right)^2\right] \quad (9)$$

Substituting the water influx term from Equation 9 into the gas material balance in Equation 8, we obtain:

$$\frac{p}{Z}\approx\frac{p_i}{Z_i}\left[1-(1-\alpha)\left(\frac{G_p}{G}\right)+(\beta-\alpha)\left(\frac{G_p}{G}\right)^2-\beta\left(\frac{G_p}{G}\right)^3\right] \quad (10)$$

One possible benefit of the cubic material balance formulation is the algebraic manipulation of the p/Z – G_p^3 model to yield a direct calculation of the water influx function (W_e) (Blansigame and Zonoozi, 2005):

$$W_e=\frac{GB_{gi}}{B_w}\left[1-\frac{1}{\left[1-(1-\alpha)\left(\frac{G_p}{G}\right)+(\beta-\alpha)\left(\frac{G_p}{G}\right)^2-\beta\left(\frac{G_p}{G}\right)^3\right]}\right]\left[1-\frac{G_p}{G}\right] \quad (11)$$

Applying this calculation requires that the p/Z-G_p^3 expression be calibrated to get α and β to a specific data set. The calibration will be done using a subroutine for solver function and also using a tool for data analysis called type curve solution.

Havlena and Odeh interpretation

Neglecting water expansion and pore compaction, the material balance equation for gas reservoirs subjected to water influx can be expressed as Alattar (2009):

$$\frac{F}{E_g}=G+\frac{W_eB_w}{E_g} \quad (12)$$

where the terms F and E_g is defined by:

(1) Underground Fluid withdrawal F:

$$F=G_pB_g+W_pB_w \quad (13)$$

(2) Gas expansion E_g:

$$E_g=B_g-B_{gi} \quad (14)$$

Using the production, pressure and PVT data, the left side of expression (Equation 12) should be plotted as a function of cumulative gas production, G_p. This is simply for display purposes to inspect its variation during depletion. If the reservoir is affected by natural water influx, the plot of F/E_g will usually produce concave downward shaped arc whose exact from is dependent upon the aquifer size and strength (Alattar, 2009).

Equation 12 can be interpreted as a linear function. Once a straight line has been achieved, based on matching observed production and pressure data, it shows that a suitable mathematical model to describe the performance of the reservoir has been found (Dake, 2001) and the interception in ordinate axis gives us the value of GIIP.

MATERIALS AND METHODS

In this work, we will consider an edge infinite acting aquifer with

Table 1. Superposition matrix for water influx calculation (time vs. pressure steps).

Time step	1	2	3	4	5	6	7	8	9	10	11	12	13	14	15	16	17
Δp_1	W_{D1}	W_{D2}	W_{D3}	W_{D4}	W_{D5}	W_{D6}	W_{D7}	W_{D8}	W_{D9}	W_{D10}	W_{D11}	W_{D12}	W_{D13}	W_{D14}	W_{D15}	W_{D16}	$W_{D..}$
Δp_2		W_{D1}	W_{D2}	W_{D3}	W_{D4}	W_{D5}	W_{D6}	W_{D7}	W_{D8}	W_{D9}	W_{D10}	W_{D11}	W_{D12}	W_{D13}	W_{D14}	W_{D15}	$W_{D..}$
Δp_3			W_{D1}	W_{D2}	W_{D3}	W_{D4}	W_{D5}	W_{D6}	W_{D7}	W_{D8}	W_{D9}	W_{D10}	W_{D11}	W_{D12}	W_{D13}	W_{D14}	$W_{D..}$
Δp_4				W_{D1}	W_{D2}	W_{D3}	W_{D4}	W_{D5}	W_{D6}	W_{D7}	W_{D8}	W_{D9}	W_{D10}	W_{D11}	W_{D12}	W_{D13}	$W_{D..}$
Δp_5					W_{D1}	W_{D2}	W_{D3}	W_{D4}	W_{D5}	W_{D6}	W_{D7}	W_{D8}	W_{D9}	W_{D10}	W_{D11}	W_{D12}	$W_{D..}$
Δp_6						W_{D1}	W_{D2}	W_{D3}	W_{D4}	W_{D5}	W_{D6}	W_{D7}	W_{D8}	W_{D9}	W_{D10}	W_{D11}	$W_{D..}$
Δp_7							W_{D1}	W_{D2}	W_{D3}	W_{D4}	W_{D5}	W_{D6}	W_{D7}	W_{D8}	W_{D9}	W_{D10}	$W_{D..}$
Δp_8								W_{D1}	W_{D2}	W_{D3}	W_{D4}	W_{D5}	W_{D6}	W_{D7}	W_{D8}	W_{D9}	$W_{D..}$
Δp_9									W_{D1}	W_{D2}	W_{D3}	W_{D4}	W_{D5}	W_{D6}	W_{D7}	W_{D8}	$W_{D..}$
Δp_{10}										W_{D1}	W_{D2}	W_{D3}	W_{D4}	W_{D5}	W_{D6}	W_{D7}	$W_{D..}$
Δp_{11}											W_{D1}	W_{D2}	W_{D3}	W_{D4}	W_{D5}	W_{D6}	$W_{D..}$
Δp_{12}												W_{D1}	W_{D2}	W_{D3}	W_{D4}	W_{D5}	$W_{D..}$
Δp_{13}													W_{D1}	W_{D2}	W_{D3}	W_{D4}	$W_{D..}$
Δp_{14}														W_{D1}	W_{D2}	W_{D3}	$W_{D..}$
Δp_{15}															W_{D1}	W_{D2}	$W_{D..}$
Δp_{16}																W_{D1}	$W_{D..}$
$\Delta p..$																	$W_{D..}$

radial flow. The data used is from an unknown field, and adopted from Dake (2001) to be used for the two comparative models.

van Everdingen-Hurst model

The unsteady state model of van Everdingen-Hurst is the most accurate method for predicting water influx. It gives results near to what can be obtained by having real field data (Ahmed, 2005).

Computing water influx using van Everdingen and Hurst, is obtained through the following steps (Agarwal, 1967; Ahmed, 2005; Alattar, 2009):

Step 1: Determine the water influx constant U or B [bbl/psi], using Equation 2.
Step 2: Calculate the corresponding dimensionless time, for each time period, using Equation 3.
Step 3: Determine the dimensionless water influx W_{eD} or W_D, using Edwardson expression, Equations 4, 5 and 6.
Step 4: Calculate the cumulative water influx [bbl], using Equation 1.

In calculating the cumulative water influx into a reservoir at successive intervals, it is necessary to calculate the total water influx from the beginning.

The pressure drop Δp, for each time step is calculated using Timmerman and McMahon approximation (Dake, 2001).

The van Everdingen and Hurst model uses the superposition principle for computing water influx.
Therefore, to calculate the cumulative water influx W_e at some arbitrary time t, which corresponds to the end of the n^{th} time step, requires superposition of the solutions of, Equation 1, to give:

$$W_e(t) = B\left[\Delta P_o W_D(t_D) + \Delta P_1 W_D(t_D - t_{D1}) + \cdots + \Delta P_j W_D\left(t_D - t_{Dj}\right) + \cdots + \Delta P_{n-1} W_D(t_D - t_{Dn-1})\right]$$

This means that the complex expression for Equation 1, can simply be evaluated as the scaler or dot product, presented in Table 1.

Finally, the cumulative water influx for each time step using matrix form is calculated by:

$$W_e = B\sum \Delta p W_D \tag{15}$$

New p/Z-G_p^3 cubic cumulative production model for the water influx

Computing water influx using the cubic cumulative model of Agarwal, is obtained through the following steps (Agarwal, 1967; Ahmed, 2005; Alattar, 2009; Blansigame and Zonoozi, 2005):

Step 1: Verification of quadratic behavior of p/Z vs. G_p, presented in Equation 9.
Step 2: Calibrate the two unknown parameters, α and β, using type curve or solver solution.

Type curve solution

The type curve [5] solution will be used to help in calibration to get α and β.

(a) Observed data is plotted using an appropriate format: Using the observed data, we plot a graph P_D vs G_p/G using the Equations 17 and 18. The calibration is done using the type curve solution and also by a subroutine developed for solver function.
(b) A "match" is found between observed data and a dimensionless solution by sliding the data plot over the type curve plot. In this step, different combination for α and β is done. The best values is considered as the good match between observed data a dimensionless solution acquired using Equation 19.
(c) The "match" is used to determine model parameters for the observed data.

For that, the p/Z-G_p^3 in Equation 10 can be rearranged to yield:

$$\left[1 - \frac{p}{Z}\frac{Z_i}{p_i}\right] \approx \left[(1-\alpha)\left(\frac{G_p}{G}\right) - (\beta-\alpha)\left(\frac{G_p}{G}\right)^2 + \beta\left(\frac{G_p}{G}\right)^3\right] \tag{16}$$

Table 2. Superposition matrix, for water influx calculation.

Pressure drop/Time step	0.25	0.50	0.75	1.00	1.25	1.50	1.75	2.00	2.25	2.50	2.75	3.00	3.25	3.50	3.75	4.00	4.25	4.50	...
Δp_1	61.99	160.89	252.90	332.83	406.30	475.53	541.67	605.42	667.25	727.47	786.33	844.01	900.65	956.38	1011.27	1065.42	1118.89	1171.73	1224.00	...
Δp_2	120.59		312.99	491.98	647.49	790.42	925.09	1053.76	1177.78	1298.05	1415.21	1529.72	1641.93	1752.12	1860.53	1967.32	2072.66	2176.68	2279.48	...
Δp_3	110.65			287.19	451.43	594.11	725.26	848.83	966.89	1080.69	1191.04	1298.54	1403.61	1506.57	1607.68	1707.15	1805.14	1901.80	1997.24	...
Δp_4	111.57				289.56	455.15	599.02	731.25	855.84	974.87	1089.61	1200.88	1309.27	1415.20	1519.01	1620.96	1721.25	1820.05	1917.50	...
Δp_5	116.10					301.32	473.65	623.36	760.96	890.62	1014.49	1133.89	1249.68	1362.47	1472.71	1580.74	1686.83	1791.20	1894.01	...
Δp_6	108.38						281.29	442.15	581.91	710.36	831.39	947.03	1058.49	1166.58	1271.87	1374.78	1475.62	1574.66	1672.08	...
Δp_7	103.72							269.18	423.12	556.86	679.79	795.61	906.27	1012.94	1116.38	1217.14	1315.62	1412.12	1506.89	...
Δp_8	103.67								269.05	422.92	556.60	679.47	795.24	905.84	1012.46	1115.85	1216.56	1314.99	1411.45	...
Δp_9	98.63									255.98	402.38	529.56	646.46	756.61	861.84	963.28	1061.65	1157.46	1251.12	...
Δp_{10}	90.20										234.11	368.00	484.32	591.23	691.96	788.21	880.97	970.94	1058.57	...
Δp_{11}	85.03											220.68	346.89	456.53	557.31	652.26	742.99	830.43	915.23	...
Δp_{12}	83.21												215.95	339.45	446.75	545.36	638.28	727.06	812.63	...
Δp_{13}	81.35													211.13	331.87	436.76	533.18	624.02	710.81	...
Δp_{14}	77.71														201.68	317.01	417.21	509.31	596.09	...
Δp_{15}	74.68															193.82	304.66	400.96	489.47	...
Δp_{16}	72.48																188.10	295.68	389.13	...
Δp_{17}	70.56																	183.13	287.86	...
Δp_{18}	74.72																		193.92	...
...	...																			...

Defining: Dimensionless pressure and dimensionless cumulative gas produced as:

$$p_D \approx \left[1 - \frac{p}{Z}\frac{Z_i}{p_i}\right] \tag{17}$$

$$G_{pD} \approx \left[\frac{G_p}{G}\right] \tag{18}$$

Which yields the final dimensionless form:

$$p_D \approx (1-\alpha)G_{pD} - (\beta-\alpha)G^3{}_{pD} + \beta G^3{}_{pD} \tag{19}$$

Step 3: Calculate the cumulative water influx [bbl], using Equation 11.

RESULTS AND DISCUSSION

Water influx using the van Everdingen and Hurst model

The pressure drop Δp, for each time step is calculated using van Everdingen, Timmerman and McMahon (Ahmed, 2005) approximation.

For dimensionless water influx W_D, we used the Edwardson et al. (1962) polynomial expressions, presented in Equations 4, 5 and 6.

Thus, we get the dimensionless time t_D, pressure drop Δp and dimensionless water influx W_D. Then, we elaborate the superposition matrix presented in Table 2.

The water influx for each time step is given by Equation 1. The results of computation of water influx are presented in Table 3.

Water influx using the cubic cumulative model

First, we prove the quadratic behavior presented in Equation 9. This is as shown in Figure 2. This gives us Equation 9 in the following form:

$$\frac{1}{\left[1 - \frac{W_e B_w}{G B_{gi}}\right]} = 0.1753\left(\frac{G_p}{G}\right)^2 + 0.0128\left(\frac{G_p}{G}\right) + 1.0012 \tag{20}$$

This relation proves the quadratic behavior of Equation 9. The values of α and β needs to be calibrated in order to compute the water influx by using Equation 11.

In order to use Equation 11 to computer water influx, there is a need of calibrating the cubic cumulative model ($p/z - G_p{}^3$).

Table 3. Water influx for each time step.

Time t (Years)	Dimensionless Time, t_D	Reservoir Pressure Pr (Psia)	Pressure Decrement Δp (psia)	Dimensionless Water Influx W_D	Water Influx We (MMrb)
	-	4,090.00			0.00
0.25	2.05	3,966.02	61.99	2.595	1.95
0.5	4.09	3,848.81	120.59	4.080	5.44
0.75	6.14	3,744.71	110.65	5.369	9.18
1	8.18	3,625.68	111.57	6.554	14.58
1.25	10.23	3,512.51	116.10	7.671	22.24
1.5	12.28	3,408.92	108.38	8.738	30.38
1.75	14.32	3,305.08	103.72	9.766	39.35
2	16.37	3,201.58	103.67	10.764	49.16
2.25	18.42	3,107.82	98.63	11.735	61.10
2.5	20.46	3,021.17	90.20	12.685	74.10
2.75	22.51	2,937.76	85.03	13.615	84.90
3	24.55	2,854.76	83.21	14.529	99.41
3.25	26.60	2,775.06	81.35	15.428	116.15
3.5	28.65	2,699.35	77.71	16.313	134.41
3.75	30.69	2,625.71	74.68	17.187	149.84
4	32.74	2,554.39	72.48	18.050	166.31
4.25	34.79	2,484.58	70.56	18.902	182.71
4.5	36.83	2,404.96	74.72	19.745	201.16
4.75	38.88	2,323.46	80.56	20.580	219.17
5	40.92	2,241.88	81.54	21.406	236.22
5.25	42.97	2,165.70	78.88	22.225	256.40
5.5	45.02	2,093.18	74.35	23.037	277.42
5.75	47.06	2,026.30	69.70	23.843	295.71
6	49.11	1,966.36	63.41	24.642	315.84
6.25	51.16	1,904.20	61.05	25.435	337.84
6.5	53.20	1,838.56	63.90	26.223	358.58
6.75	55.25	1,772.97	65.62	27.006	375.14
7	57.29	1,700.85	68.86	27.783	393.69
7.25	59.34	1,644.98	64.00	28.556	412.61
7.5	61.39	1,596.83	52.01	29.324	429.67
7.75	63.43	1,548.80	48.09	30.088	443.54

The calibration is done using type curve solution and also by a subroutine developed for solver function.

Type curve solution

The type curve solution, presented in Figure 3, gives a better match for combination of α and β, as illustrated in Table 4.

Solver function

A subroutine using VBA-Visual Basic for Applications-2013 was developed for a solver function, in order to get the best approximation values for α and β as illustrated in Table 5.

The 2 (two) presented workflows allows the computation of water influx using the van Everdingen-Hurst and the cubic cumulative production model of Agarwal. The comparison of results is illustrated in Figure 4.

The results demonstrate clearly that the correlation between both methods depends on the calibration of the two unknown parameters α and β, appearing in the cubic cumulative model (Blansigame and Zonoozi, 2005).

Under this assumption the cubic cumulative production model with an approximation values of α =0.020573 and β =0.173889, results in a perfect match between the van Everdingen-Hurst model. Using this approximation for the unknown parameters α and β, the Havlena-Odeh (Dake, 2001) plot method in history matching, was perfomed and reservoir-aquifer performance is as shown in Figure 5.

The full Havlena and Odeh, from Equation 12, illustrated

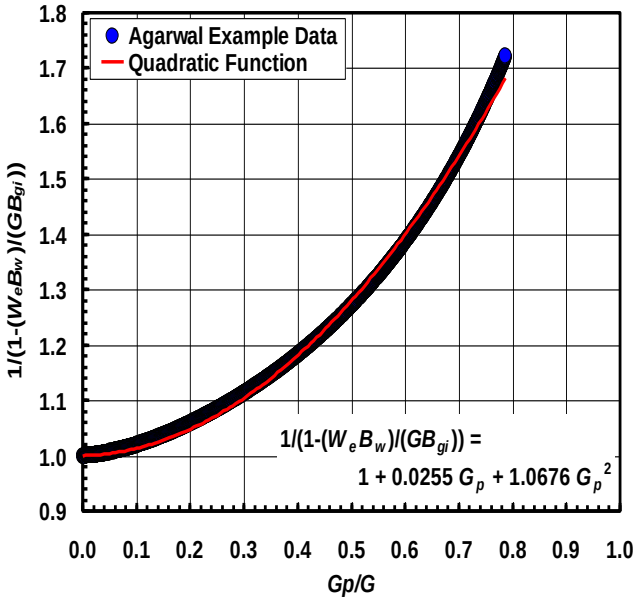

Figure 2. Quadratic behavior of "Water Influx" vs. G_p/G. Blansigame and Zonoozi (2005)

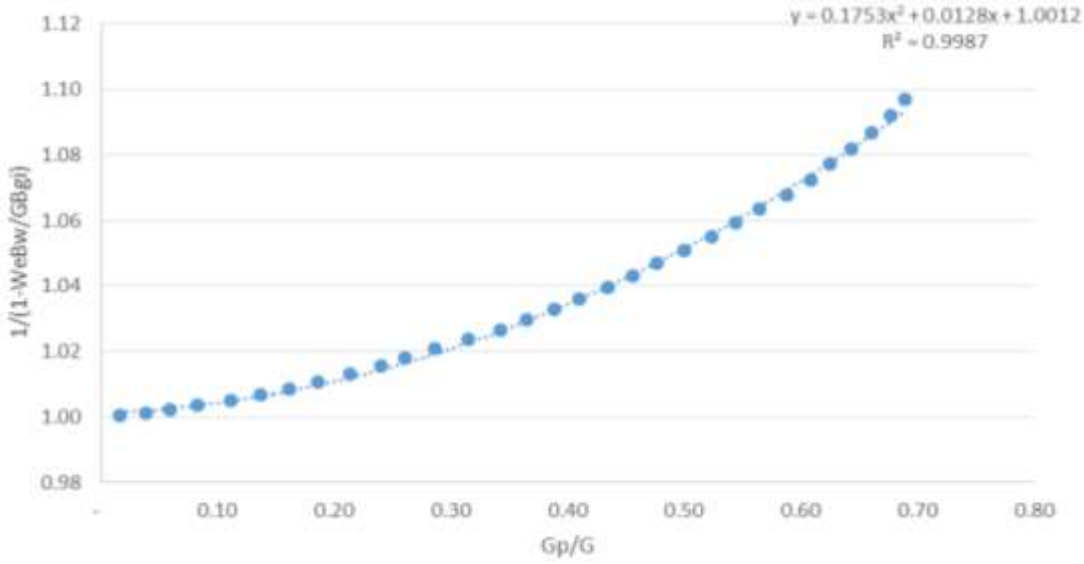

Figure 3. Approximation proof (Quadratic Behavior).

Table 4. Values of α and β using type curve solution.

Approximation	α	β
I	0.055447	0
II	0.00069	0.201177
III	0.10636	0.22986
IV	0.25	0
V	0.01008	0.166654

Table 5. Values of α and β using solver function. (by the Author: using VBA Code-2013 in Esxel spreadsheet).

Approximation	α	β
I	0.010086	0.166654
II	0	0.203711
III	0.015164	0.147997
IV	0.00069	0.201177
V	0.020573	0.173889

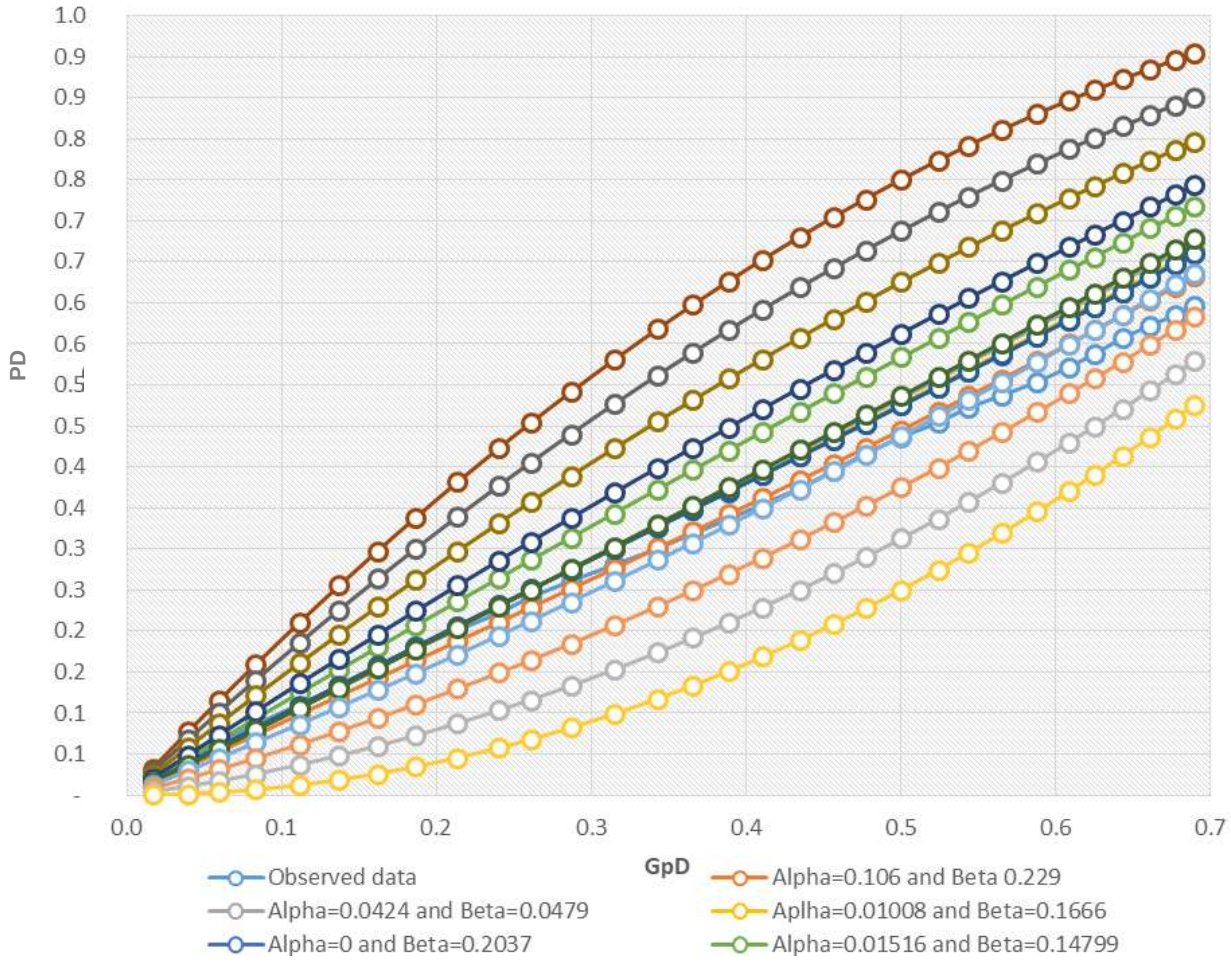

Figure 4. Type curve match for different values of α and β.

in Figure 6 shows that a correct water influx model was found, and the interception in ordinate axis gives us an approximate value of Gas Initially In Place (GIIP) of 1117 Bscf, which is identical with the correct value 1116 Bscf. This finding is aligned with the results obtained by Dake (2001). The improved material balance method demonstrated the hazards of not taking into account the influence of water influx in P/Z plots, as it can leads in overestimation of GIIP and this can have serious economic consequences for the project.

Conclusions

In this work, two workflows for computing water influx was presented.

The first workflow was for the van Everdingen-Hurst method which requires the use of the superposition

Figure 5. Comparison between van Everdingen-Hurst and cubic cumulative production model for different values of α and β.

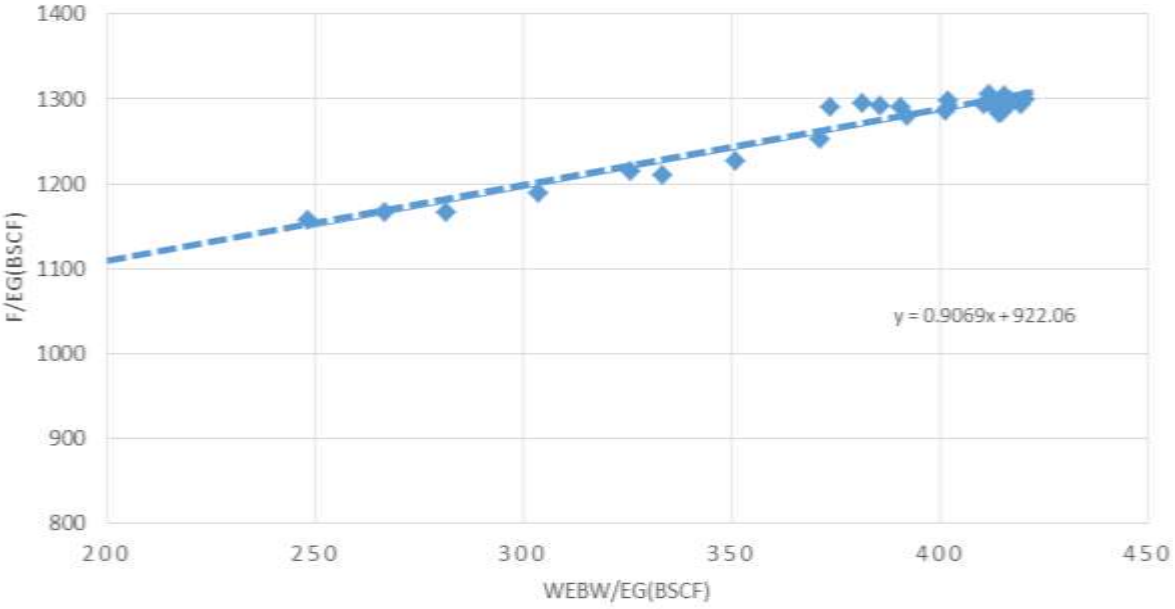

Figure 6. Application of the Havlena-Odeh plot in history matching reservoir-aquifer performance.

principle in order to find the cumulative water influx for each time step. For that reason a superposition matrix was created and the values of dimensionless water influx W_D was calculated using the Edwardson polynomials expressions.

The second workflow was for the cubic cumulative production model of Agarwal, in which there was a need of correct calibration of the unknown parameters α and β. In order to determine those parameters, two solutions were proposed. One is the type curve solution and the other one was the solver function. The most accurate solution was found for an approximation values of α

=0.020573 and β =0.173889. This solution was introduced in the derived equation for computation of water influx, presented by Blansigamen and Zonoozi (2005).

The results of cumulative water influx using cumulative production model of Agarwal was included in the generalized material balance for gas reservoirs using the Havlena and Odeh technique and a well matched solution was obtained.

The successful comparison between both methods demonstrated that it depends on the values of the unknown parameters α and β, appearing in Agarwal's model.

The results obtained in this work could be useful for industrial applications of the material balance for dry gas under influence of an infinite active aquifer. It will improve the computation of cumulative water influx using production data obtained in a reservoir, resulting in a more accurate estimation of GIIP.

CONFLICT OF INTERESTS

The authors have not declared any conflict of interests

ACKNOWLEDGEMENT

The authors are grateful to professors Luis Helder Lucas and Pal Skalle for their contribution in this topic.

REFERENCES

Agarwal R (1967). Unsteady-State Perfomance of Water-Drive Gas Reservoirs. PHD Dissetation. USA. Graduate College of the Texas A&M University: pp 8-39

Ahmed T (2005). Advanced Reservoir Engineering. Oxford OX2 8DP, UK: Elsevier Inc: pp 159-185

Alattar H (2009). Guidelines for Developing Gas Fields Associated With Edge-Water Drive. Nova Science Publishers, Inc. pp 1-30.

Blansigame T, Zonoozi N (2005). Simplified Model . Simplified Model for the Material Balance of Gas Reservoirs Experiencing Water Influx ("Cubic Cumulative Production"). Texas, USA. pp 1-24.

Dake L (2001). The Practice of Reservoir Engineering. Amsterdan : Elsevier Science B.V. pp 473-505.

Edwardson MJ, Girner HM, Parkison HR, Williams CD, Matthews CS (1962). Calculation of formation temperature disturbances caused by mud circulation. Journal of Petroleum Technology 14(04):416-426.

Feng X, Zhong B, Yang X, Deng H (2015). Effective water influx in gas reservoir development: problems and countermeasures. Elsevier pp. 240-246.

Istiak H, Mazumder SH, Mahmud H (2016). Dynamic Material Balance Study of Gas Reservoir Using Production Data: A Case Study of New Gas Sand of Kailashtila Gas Field. International Journal of Oil, Gas and Coal Engineering 4(4):38-44.

Marques JB, Trevisan OV (2007). Classic Models of Calculation of Influx: A Comparative Study. Society of Petroleum Engineers. Latin American & Caribbean Petroleum Engineering Conference, 15-18 April, 2007. Buenos Aires, Argentina. doi:10.2118/107265-MS

Shimada M (2009). Predicting Water Influx from Common Aquifers. EUROPEC/EAGE Conference and Exhibition, 1-20. doi:10.2118/120897-MS

van Everdingen A, Hurst W (1949). The Application of the Laplace Transformation to Flow Problems in Reservoirs. Journal of Petroleum Technology 1(12):305-324.

Vol. 10(4), pp. 65-70, July-September 2019
DOI: 10.5897/JPGE2019.0316
Article Number: 5257C6D61763
ISSN: 2I41-2677

http://www.academicjournals.org/JPGE

ACADEMIC JOURNALS
expand your knowledge

Journal of Petroleum and Gas Engineering

Full Length Research Paper

Concept of complete CO_2 capture from natural gas inside exploration wells and its storage in rock reservoirs

Marco Ludovico-Marques

INCITE, Polytechnic Institute of Setúbal, Barreiro School of Technology, Portugal.

Received 26 February, 2018; Accepted 26 March, 2018

The innovative concept herein shown intends to present a new system of carbon capture and storage (CCS) from natural gas extracted on cement completions of gas wells by absorbent selective nanoporous materials, forming conducting channels on linked pores. CO_2 fluids will be transported upwards and then injected and stored in upper nonproductive oil and gas porous rock reservoirs by the removal-transport-injection system (RTIS), assuring also the mechanical safety of the wells. This innovative concept allows the treatment of natural gas in oil and gas wells on fields, through the extraction of carbon dioxide. The natural gas will be free of CO_2, the major responsible gas for green house effect and therefore its production will be environmentally friendly.

Key words: Carbone dioxide, carbon capture and storage (CCS), gas wells, completion, removal-transport-injection system (RTIS).

INTRODUCTION

Oil and Gas accounted close to 60% of primary energy consumption in 2017 and the gas quantity was higher than 20% (Dudley, 2019). The transition to a lower-carbon fuel mixture is ongoing, and will be guided by natural gas and renewables use towards 2040. The renewables will grow faster in the world energy system than any fuel before. Considering the rapid transition scenario (RT), the growth of the renewables will be the highest ever, with an increment between 1 and 10% in 15 years. In this scenario, oil and gas will account for almost 50% of primary energy consumption in 2040 and the gas quantity will be lower than 30%. The renewables will account only around 15% of consumption in spite of the prediction of its strong growth. The consumption of oil will decrease and the use of gas will continue to increase, helped by the contribution of the growing use of carbon capture use and storage (CCUS) in the RT scenario. The quantity of natural gas use in 2040, in conjunction with CCUS, will be about 1/3 of the total consumption amount (Dudley, 2019).

The development of materials with high availability for CO2 capture and storage (CCS), retention capacity and absorption selectivity it is a quest in science and technology nowadays. Many materials are being investigated in order to correspond to this major challenge, encompassing factors as: availability, environmental friendliness, non-toxicity, a low level of greenhouse gas emission during processing, material

E-mail: ludovicomarques@gmail.com, marco.marques@estbarreiro.ips.pt. Tel: 212064660. Fax: 212075002.

stability, production cost, energy of adsorption/ desorption, sorbent regeneration, sorption kinetics and capacity per volume or per mass of host material (Cavalcanti et al., 2018).

Cavenati et al. (2004) stated that the adsorption is a main unit operation in the chemical and petrochemical industries in order to carry out separation and purification of gas mixtures, namely in the case of the methane-carbon dioxide. The carbon dioxide capture from a gas mixture flue can be done by selective efficient adsorbents as zeolites. They referred also the CO_2 and N_2 removal from natural gas streams through proper adsorbents by the Molecular Gate technology (Engelhard, USA).

Joos et al. (2015) reported that the exhaust gases with a residual heat at 400 K are sent into the atmosphere under a high-pressure stream after leaving the heat exchanger of a fossil fuel-fired power plant. In the context of CCS, on nanoporous materials, the CO_2 adsorption can be favored by the differences in the entropy and adsorption enthalpy for CO_2 and H_2O at high temperature, and H_2O absorption at low temperature. The adsorption of CO_2 is carried out at high temperature (400 K), and the release of CO_2 occurs at low temperature, being the absorbent saturated with H_2O.

Joos et al. (2015) also referred advantageous materials aside zeolites and zeolitic imidazolate frameworks (ZIFs), e.g. metal-organic frameworks (MOFs), and porous polymer networks (PPNs). Other authors reported procedures to carry out the carbon dioxide sequestration and separation from gas mixtures (Rolniak and Kobayashi, 1980; Sircar, 1988; Dong et al., 1998; Talu, 1998; Dreisbach et al., 1999; Murata and Kaneko, 2000, Siriwardane et al., 2001; Siperstein and Myers, 2001; Krooss et al., 2002; Murata et al., 2002; Ko et al., 2003; Olajossy et al., 2003). This paper aims to present the concept of an advanced innovation in Oil and Gas industry: the CO_2 capture from natural gas mixtures inside moderate and deep gas wells and its storage in upper nonproductive porous rock formations.

This innovative concept herein shown intends to avoid the extraction of carbon dioxide from gas wells and its lifting and transport to surface Oil and Gas facilities on fields. The natural gas will release carbon dioxide through well cement completions that will be injected and stored in upper nonproductive Oil and Gas porous rock reservoirs, assuring the mechanical safety of the wells.

MATERIALS AND METHODS

The Oil and Gas wells comprise near surface or intermediate or deep well bores with cement in annulus between rock walls, covered with mud support, and steel casings (API Spec 7-1/ISO 10424-1 (2004, 2007, 2009, 2011), TR 5C3/ISO 10400 (2007, 2015), ISO 10426-1 ANSI/API SPECIFICATION 10A (2009), API RP96 (2013)). A representative production steel casing is herein described with $9^{5/8}$ in. O.D., surrounded by a typical cement thickness of 1.5 in. on the referred annulus and encompassing an inner production tubing or liners. The communication between the rock reservoir and the well is carried out by casing perforating explosives, blasted inside the well that allow the flow of natural gas from the reservoir to the production well.

According to Cavenati et al. (2004), the natural gas is composed mainly of methane, between circa 80 and 95%, with variable amounts of C_{2+} hydrocarbons and nitrogen, carbon dioxide as a minor component (around 1%). However, the effluent gas extracted from a well under a CO_2 flooding may contain 20 to 80% of CO_2.

CO_2 injection and storage in rock reservoirs is a common practice in Oil and Gas industry. The modeling studies required to increase its performance are very important (Salem and Shedid, 2013).
Also, in order to prevent the equipment and pipeline corrosion, the carbon dioxide reduction has a major importance.

Carbon dioxide is supercritical in gas reservoirs generally at depths higher than 1 km and at temperatures higher than 35°C. According to Vargaftik (1975), the phase diagram shows the critical point at P = 73.8 bar (P = 7.4 MPa) and T = 31.0°C. Therefore, carbon dioxide has supercritical and gaseous states. Supercritical carbon dioxide is a fluid with hydrostatic gradient value of 0.091 bar/m approaching that value of water. However, pure carbon dioxide gas value of viscosity is circa 0.015 cP (1.5×10^{-5} Pa.s) at 61 bar and 40°C, higher than pure methane value of viscosity at same P and T that is about 0.011 cP, showing low viscosity. These values of viscosity increase around ten times at 101 bar and same temperature. Even supercritical carbon dioxide reveals high mobility.

Most demanded well cements are ISO/API classes C, D, G, H and are intended for use when conditions require high, early strength and are available in moderate sulphate-resistant (MSR) and high sulphate-resistant (HSR) grades, similar to ASTM C150, type III (ISO 10426-1 ANSI/API SPECIFICATION 10A (2009)).

According to ISO 10426-1 ANSI/API SPECIFICATION 10A (2009), the ground clinker generally consists of hydraulic calcium silicates, aluminates and usually contains one or more forms of calcium sulfate as an interground additive. During manufacture of class G and H well cements, aside calcium sulfate or water, or both, no additives are allowed to be intergrounded or blended with the clinker. The main standard chemical composition of these cements is the following: maximum value of 6% of magnesium oxide and 3-3.5% of sulfur trioxide (3.5% class C), tricalcium silicate varying between 48% and the extremes 58% (MSR) - 65% (HSR), tricalcium aluminate with the maximum values of 3% (HSR)-8% (MSR), tetracalcium aluminoferrite has the maximum value of 24% (HSR). The total alkali content expressed as sodium oxide equivalent has the maximum value of 0.75%.
The maximum values of the insoluble residue and the loss on ignition are 0.75 and 3%. The free-fluid content has the maximum of 5.9% on G and H and the mixture water values are the following: 56% on C, 38% on D, 44% on G, 38% on H.

The compressive strength tests are obtained after 8 h or after 24 h of curing time. These tests can be carried out, the both, under atmospheric pressure on C, G and H or 20.7 MPa (3000 psi) pressure on D. The compressive strength values obtained on C, G, H specimens are shown in Table 1. D specimens should have compressive strength values of 3.4 MPa (500 psi) and 13.8 MPa (2000 psi) after final curing times of 8 and 24 h at a temperature of 110°C (230°F). After a final curing time of 24 h at a temperature of 77°C (170°F), the compressive strength values on D specimens should be 6.9 MPa (1000 psi). The cement class G has a major use on completion works in moderate and deep wells constructed in the world. The porosity and permeability data of the cement class G are herein analyzed under degradation effect of carbon dioxide saturated water and supercritical carbon dioxide, based on an experimental simulation case of a completion inside a gas well.

Um et al. (2011) conducted an experiment on 14 mm diameter × 90 mm long samples of a class G cement with w/c = 0.33 (water/cement ratio). These specimens were tested under the temperature of 50°C and a pressure of 10 MPa in order to represent the CO_2 injection's temperature and pressure conditions

Table 1. Compressive strength values obtained on C, G, H API classes.

Values of compressive strength of API classes C, G, H (MPa)		
Curing time (hours)	8	
Curing temperature (ºC)	38	60
Compressive strength (MPa)	2.1	10.3
Curing time (hours)	24	
Curing temperature (ºC)	38	60
Compressive strength (MPa)		
C	13.8	No requirement
G and H	No requirement	No requirement

at 1 km of depth, a geothermal gradient of 30°C/km and a pressure gradient of 10.5 MPa/km. These samples shown a degradation depth of circa 1 mm after 1 month of testing and around 3.5 mm after 5 months, whereas the carbonated cement shown on the outer degraded zone increased the porosity and cracks occurrence, developing mainly nano-meter sized pores lower than 20 nm.

The air permeability of cement samples was predicted to increase, according to Ghabezloo et al. (2009) porosity-dependent equation, from 0.58 to 34.74 mD (34.74×10^{-15} m^2) after 1 month reaction with CO_2 saturated water at high P-T, as a result of porosity increment from 31 to 45%. The results obtained by Um et al. (2011) revealed that the degradation effect of CO_2 saturated groundwater was higher than the effect of cement exposure to supercritical CO_2, according to X-ray microtomography images carried out on deteriorated specimens.

Gasda et al. (2004) also referred the potential leakage of CO_2 occurrence on the interface between host rock and cement, cement and casing, cement plug and casing, or through the cement pore space and fracture.

THE INNOVATIVE CONCEPT

The cement material used by completion procedures should encompassing carbon dioxide selective absorbent nanoporous materials, capable of removing carbon dioxide from natural gas-rich methane mixtures flowing from reservoir rocks, under high pressures and temperatures inside the wells, after the curing time of 24 h, as super critical carbon dioxide. Then, this fluid is conducted through the main micro and nanopores channels of linked nanoporous materials on cements, physically and mechanically adequate for this purpose, towards less warm upper levels. The mechanical behavior of ISO/API cements improved by this construction procedure should be, aside compression resistance, both tensile resistant to inner circulation of carbon dioxide and ductile enough to accommodate variations of annulus deformation caused by rock walls displacements.

Several embedded and linked extraction micro devices will exert capillary forces and/or suction pressures responsible for this uplift phenomenon. These should be linked to compressor micro devices included on cement top levels that will receive and develop carbon dioxide deeper injections into upper non-productive porous rock formations. This system of removal-transport-injection (RTIS) inside the wells completion should have proper nanosized sensors connected to a central unit and could be machine learning guided.

Open porosity values of circa 30% of cements inside representative wells' annular sections of about 158 cm^2 that is, 24.5 $in.^2$, trough 1 km wellbore-long, means a volume higher than 4.7×10^6 cm^3 (4.7 m^3) that is, circa 560 ft^3 (cf). Considering a representative production of 5000 barrels of oil per day of 24 h (BOPD) and a GOR of 700 scf/bbl (Jacobsen et al., 1990), that is, 3.5×10^6 scf of natural gas per day. Assuming a composition of carbon dioxide of 1%, gives 3500 scf. This means, that in this case the RTIS will perform more than 6 travels of carbon dioxide upwards per day on cement completion, that is, a travel per less than 4 h or circa 7 cm/s (0.7 m/s or 2.75 in./s). Figure 1 illustrates the general working methodology of RTIS in a well gas. This innovative concept could also consider thinner vertical transport tubes, manufactured with e.g. shape metallic alloys, inside cement completion to carry out carbon dioxide but would require to tackle with expected corrosion problems that could occur caused by e.g. H_2S. This phenomenon will jeopardize the uplift of carbon dioxide, the physical and mechanical stability of completion and the support effect of casings in Oil and Gas wells.

DISCUSSION

Ghabezloo et al. (2009) shown based on permeability determined on 90°C-cured and saturated class G cement samples carried out inside triaxial tests chambers, the availability of inducing transient pulse from differential pressure applied on both ends of the specimens with 76 mm of length. The specimens were under an effective stress inside the pore space of the cement of circa 12 MPa, obtained from the difference between the value of 30 MPa of external confining oil's hydrostatic pressure and 18 MPa of the value of the internal pore pressure fluid. It took about two hours to reach the value of 7.5 Mpa from the initial pore pressure of circa 18 MPa, recorded between the two opposite ends of the 76 mm-long

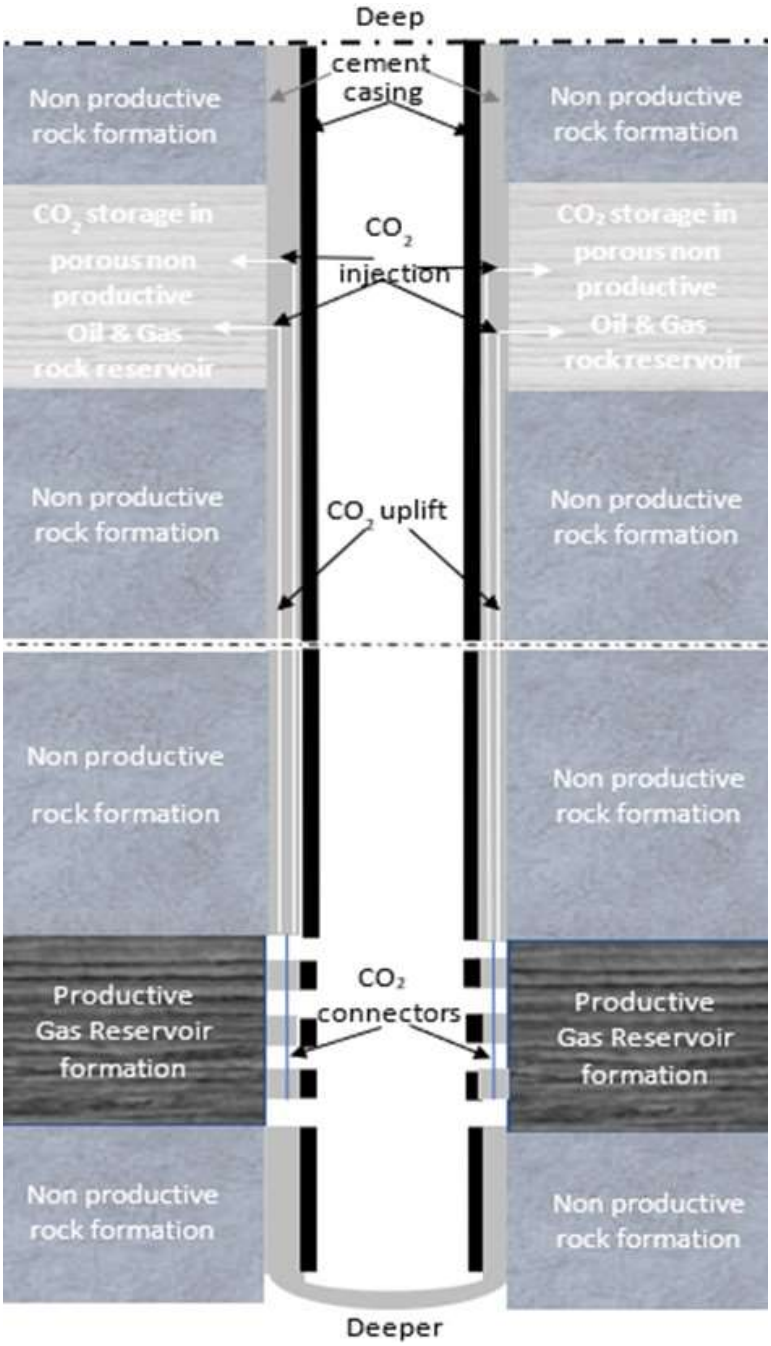

Figure 1. General working methodology of RTIS in a well gas.

specimens. The radial strain value obtained under the former pore pressure was circa 8×10^{-4}. The confining stress applied on the specimen was 22.5 MPa.

These data are an evidence of the availability of inducing supercritical fluid flow inside pores of cement materials at pressures similar to those that occur at more than 1 km depth without mechanical failure. However, the experimental evidence shown a significative difference between the referred velocity of travel of supercritical CO_2 of 0.7 m/s and the velocity value of 0.38 m/h obtained by Ghabezloo et al. (2009) on water transport. The viscosity of the supercritical CO_2 is circa ten times lower than the viscosity of water and contributes to the significant increment of the velocity of the travel of the former in the cement voids.

Hasan et al. (2013) studied microporous materials for sorbents capable of capturing and compressing atmospheric CO_2 with low cost and high purity and

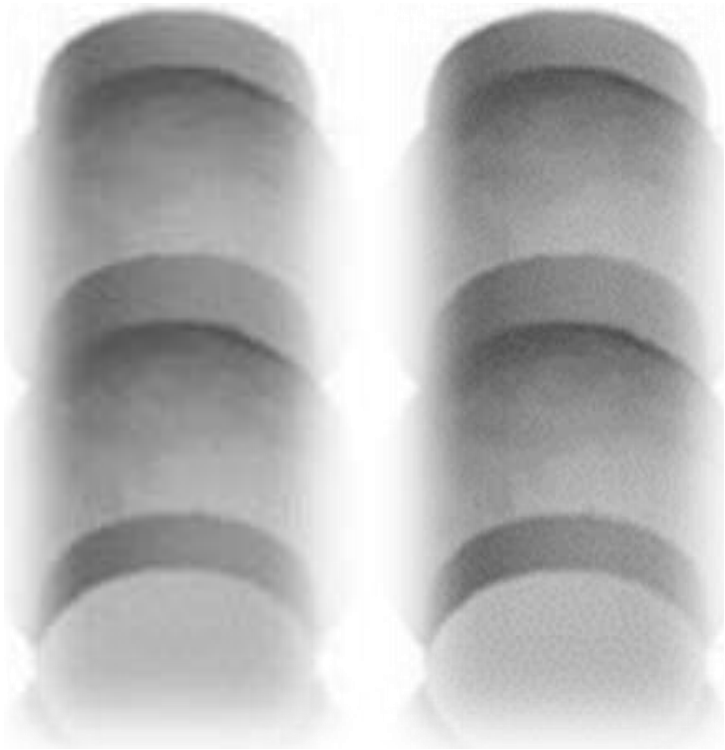

Figure 2. Model of columns of cylinders connected to spheres.

recovery, based on a computational screening approach that combines zeolites selection and process optimization. They considered a mixture-flue of 14% CO_2 and of 86% N_2 that went under adsorption in several zeolite's voids by two operational modes: pressure-swing adsorption (PSA) and vacuum-swing adsorption (VSA).

Considering the molecules of CO_2 and N_2 as hard spheres of diameter of respectively 3.4 Å and 3.1 Å, and the methane molecule with an effective length and diameter of 3.99 Å, the author of the RTIS concept selected as a valid example the case of AHT zeolites for capturing and compressing CO_2. The pore length diameter (PLD) and largest cavity diameter (LCD) of AHT zeolites are 3.4 Å and 4.6 Å. The PLD of AHT zeolites is lower than effective length diameter (ELD) of methane molecule and does not allow the former to enter inside zeolite voids. This zeolite has a purity of 90% and a recovery of 91.5%. Figure 2 shows the model of pore system distribution of AHT zeolites of columns of cylinders connected to spheres (caverns). The macro-system described by Hasan et al. (2013) has a compressor that pressurizes the dry feed gas in PSA mode. The CO_2 flow enters inside the column in VSA mode. The adsorbent zeolites are packed in multiple columns. Each column's length (L) is allowed to vary from 1 to 5 m, being the optimum length of about 1 m.

The CO_2 inside each column is affected by a cycle with the following four steps: (i) pressurization, (ii) adsorption, (iii) forward blowdown, and (iv) reverse evacuation or desorption. Additional N_2 is purged by a vacuum pump during blowdown. CO_2 is extracted through a second vacuum pump, at the lowest pressure, during evacuation. After, it is compressed to 15 MPa through a compressor train with intercooling. The desorption curves of AHT zeolites under 1 MPa of pressure and T = 25-50°C show a loading of 2.5-2.75 mol of CO_2 per kg of AHT zeolite. The energy consumption per ton of captured CO_2 based on the AHT macro-system of Hasan et al. (2013) is 124 kWh and the cost per ton of CO_2 captured and compressed to 15 MPa, including dehydration, is 33.8 USD.

First et al. (2013) evaluated the market of purification of natural gas (separation between CO_2 and methane) in 97 billion USD. The RTIS concept applied on the gas production inside wells could have a major role on the industry of purification of the natural gas.

Hasan et al. (2013) described a macro-system that is another macro-evidence of the feasibility and reliability of the RTIS concept. An advantage of this concept is the following: the CO_2 extracted should be injected on rock voids under a pressure value of at least, half of the 15 MPa referred by Hasan et al. (2013), that is, 7.5 MPa. However, it will be needed to develop micro-devices e.g. micro-compressors, micro-vacuum pumps, nano-monitoring sensors operating through machine learning and micro-satellites´ connections for the RTIS concept.

The assembly of km-long column's packs of zeolites inside cement's pore voids in Oil and Gas wells is also a challenging endeavor.

ACKNOWLEDGEMENTS

The author wishes to thank to the Polytechnic Institute of Setúbal for the support and payment of the handling fee of the manuscript.

CONFLICT OF INTERESTS

The author has not declared any conflict of interests.

REFERENCES

API Spec 7-1/ISO 10424-1 (2004, 2007, 2009, 2011). Specification for rotary drill stem elements. American Petroleum Institute.

API RP96 (2013). Deepwater well design and construction. American Petroleum Institute.

Cavalcanti L, Kalantzopoulos G, Eckert J, Knudsen K, Fossum J (2018). A nano-silicate material with exceptional capacity for CO2 capture and storage at room temperature. Scientific Reports 8:11-27.

Cavenati S, Grande C, Rodrigues A (2004). Adsorption equilibrium of methane, carbon dioxide, and nitrogen on zeolite 13X at high pressures. Journal of Chemical Engineering Data 49:1095-1101.

Dong F, Kodama A, Goto M, Hirose T (1998). Simultaneous separation of a ternary gas mixture ($_{CH4}$-CO_2-N_2) by a novel PSA process. In Fundamentals of Adsorption. Le Van D, eds. Kluwer Academic Publisher. Boston pp. 769-774.

Dreisbach F, Staudt R, Keller J (1999). High-pressure adsorption data of methane, nitrogen, carbon dioxide and their binary and ternary mixtures on activated carbon. Adsorption 5(3):215-227.

Dudley B (2019). BP energy outlook 2019 edition. United Kingdom 73 p.

ISO 10426-1 ANSI/API SPECIFICATION 10A (2009). Specification for cements and materials for well cementing/Petroleum and natural gas industries. Cements and materials for well cementing —Part 1: Specification. International Organization for Standardization/ American Petroleum Institute.

First E, Hasan M, Floudas C (2013). Computational discovery of cost-effective materials for carbon capture and other molecular separations. Computer-Aided Systems Laboratory, Princeton University. helios.princeton.edu/CO2/

Gasda S, Bachu S, Celia M (2004). Spatial characterization of the location of potentially leaky wells penetrating a deep saline aquifer in a mature sedimentary basin. Environmental Geology 46:707-720.

Ghabezloo S, Sulem J, Saint-Marc J (2009). Evaluation of a permeability-porosity relationship in a low permeability creeping material using a single transient test. International Journal of Rock Mechanics and Mining Sciences 46(4):761-768.

Hasan M, First E, Floudas C (2013). Cost-effective CO2 capture based on in silico screening of zeolites and process optimization. Physical Chemistry Chemical Physics 15:17601-17618.

Jacobsen S, Everett B, Levien L, Van Baaren C, Neuman C, Watson J (1990). Log interpretation strategies in gas wells. SPWLA 31st Annual Logging Symposium. Louisiana. USA.

Joos L, Lejaeghere K, Huck J, Speybroecka V, Smit B (2015). Carbon capture turned upside down: high temperature adsorption and low-temperature desorption (HALD). Energy Environment Science 8:2480.

Ko D, Siriwardane R, Biegler L (2003). Optimization of pressure swing adsorption process using zeolite 13X for CO2 sequestration. Industrial and Engineering Chemistry 42:339-348.

Krooss B, van Bergen F, Gensterblum Y, Siemons N, Pagnier H, David P (2002). High-pressure methane and carbon dioxide adsorption on dry and moisture-equilibrated pennsylvanian coals. International Journal of Coal Geology 51:69-92.

Murata K, Miyawaki J, Kaneko K (2002). A simple determination method of the absolute adsorbed amount for high-pressure gas adsorption. Carbon 40:425-428.

Murata K, Kaneko K (2000). Nano-range interfacial layer upon high-pressure adsorption of supercritical gases. Chemical Physics Letters 321:342-348.

Olajossy A, Gawdzik A, Budner Z, Dula J (2003). Methane separation from coal mine methane gas by vacuum pressure swing adsorption. Transactions of the Institution of Chemical Engineers 81(A):474-482.

Rolniak P, Kobayashi R (1980). Adsorption of methane and several mixtures of methane and carbon dioxide at elevated pressures and near ambient temperatures on 5A and 13X molecular sieves by tracer pertubation chromatography. American Institute of Chemical Engineers Journal 26(4):616-625.

Salem A, Shedid S (2013). Variation of petrophysical properties due to carbon dioxide (CO2) storage in carbonate reservoirs. Journal of Petroleum and Gas Engineering 4(4):91-102.

Siperstein F, Myers A (2001). Mixed-gas adsorption. American Institute of Chemical Engineers Journal 47(5): 141-1159.

Sircar S. (1988). High efficiency separation of methane and carbon dioxide mixtures by adsorption. American Institute of Chemical Engineers Symposium Series 84(264):70-72.

Siriwardane R, Shen M, Fisher E (2001). Adsorption of CO_2 on molecular sieves and activated carbon. Energy Fuels 15:279-284.

Talu O (1998). Needs, status, techniques and problems with binary gas adsorption experiments. Advances in Colloid and Interface Science 76-77:227-269.

TR 5C3/ISO 10400 (2007, 2015). Technical report on equations and calculations for casing, tubing, and line pipe used as casing or tubing; and performance properties tables for casing and tubing. American Petroleum Institute.

Um W, Jung H, Martin P, McGrail B (2011). Effective permeability change in wellbore cement with carbon dioxide reaction. Pacific Northwest National Laboratory (under contract for the United States Department of Energy).

Vargaftik N (1975). Tables on the thermophysical properties of liquids and gases, 2nd ed. John Wiley and Sons. New York.

Vol. 10(4), pp. 71-84, July-September 2019
DOI: 10.5897/JPGE2019.0310
Article Number: D330C7161765
ISSN: 2I41-2677

http://www.academicjournals.org/JPGE

ACADEMIC JOURNALS

Journal of Petroleum and Gas Engineering

Full Length Research Paper

A statistical approach to investigate oil displacement efficiency in thermal recovery techniques for heavy oil based on one-dimensional core experiment

Dong Liu*, Yan-Chun Su, Li-Zhen Ge, Ting-Hui Hu and Qin Zhu

Tianjin Branch of CNOOC Ltd., China National Offshore Oil Corporation, Tianjin 300459, China.

Received 18 March, 2019; Accepted 14 August, 2019

Precise description of displacement efficiency (E_d) is extremely important for evaluating the performance, economic effectiveness and final recovery of thermal recovery techniques. Current researches mainly focused on one-dimensional core displacement experiment, and it is difficult to obtain precise E_d beyond the range of test points. In addition, there are two ways to improve the E_d for thermal flooding: Increasing injection pore volume (PV) or raising injection temperature (T), it's hard to make decisions. In this study, the above two problems were solved by a statistical approach research. At the beginning, one dimensional core displacement experiment was carried out for hot water and steam, respectively. Then, dozens of curves and correlations about E_d varied with injection PV number and injection temperature was regressed, respectively. Based on this, the formula of E_d and PV, E_d and T for injection hot water and steam was established respectively, which makes up for the shortage of the finite test data points. Next, chart of the E_d between the PV and T was obtained. In addition, sensitivity analyses of injection rate and steam quality are discussed in this paper. Finally, the precise of the regression formula was verified by three steam flooding case of different heavy oil fields. The results indicated that, in order to get higher E_d, higher injection PV and temperature are beneficial. With the E_d chart, technicians can determine different schemes to improve oil displacement efficiency according to specific reservoir conditions. Besides, main production indexes such as oil recovery can be predicted quickly and precisely.

Key words: Fossil energy, heavy oil, displacement efficiency, thermal recovery, steam flooding.

INTRODUCTION

Oil reserves in the world can be classified into light oil, heavy oil and bitumen according to the density and viscosity (Butler, 1981). Because heavy oil and bitumen take up about 70% of the total remaining hydrocarbon resources (Alboudwarei, 2006), heavy oil has fascinated a great deal of attention and focus in the past decades (Munawar et al., 2015). As conventional oil reserves are running out and the demand for energy has been increasing day by day, the heavy oil resources play an more and more important role in crude oil reserve replacement to meet the world's future energy needs (Xiong et al., 2017a, b). Because of the high viscosity of

*Corresponding author. E-mail: liudong@cnooc.com.cn; Tel:+86 022 66500871.

the heavy oil, heavy oil dose not easily flow naturally in the reservoir, so it cannot be produced by conventional techniques (Ankit and Ajay, 2012; Wang et al., 2016; Xu et al., 2013).

Many processes of exploiting heavy oil have been developed and improved, such as water flooding, chemical flooding, thermal recovery, and microbial recovery (Sheikholeslami et al., 2016). Among a variety of enhanced oil recovery technologies, the thermal recovery technology has been widely used for heavy oil reservoirs (Khansari et al., 2014; Hou et al., 2016a, b), such as steam assisted gravity drainage(SAGD) (Yang et al., 2016), steam flooding (SF) (Zhao et al., 2013; Mahood et al., 2016) and cyclic steam stimulation (CSS) (Hou and Chen, 1997; Escobar et al., 2000; Bao et al., 2016), cyclic multi-thermal fluids stimulation (Hou et al., 2016c; Kuigian, 2018; Liu et al., 2018; Dong et al., 2014a, b; Dong et al., 2016). Nowadays, CSS and SF are known as the most widely used and mature technologies (Dong et al., 2012).

Sweep efficiency (E_v) and displacement efficiency (E_d) are essential parameters in oilfield development; they are the final determinant of oil recovery. For conventional cold production displacement, there are two ways to improve the final oil recovery. One is to increase the swept volume of the injected fluid, such as weak gel drive, stratified water injection, etc. The other is to increase the displacement efficiency within the swept volume, such as polymer flooding, high displacement ratio (amount of water injection divide the porosity volume). When the swept volume cannot be increased (for example, in the absence of new wells, and the injected water or steam has broken through the production well), the E_d needs to be improved. For E_d, predecessors have obtained some valuable research results. Water displacement efficiency mainly depends on the geologic factors and fluid properties, such as reservoir type, reservoir heterogeneity, rock wettability and crude oil viscosity. There are many researches on the effects of single factor on oil displacement and the ultimate oil displacement efficiency. Previous studies have focused on several aspects. First, a lot of research work has been done on the influence of wettability on E_d (Donaldson and Thomas, 1971; Anderson, 1987; Morrow, 1990). Because the wettability of reservoir rock is the main factor that determines the distribution position, flow state and distribution of fluid in pore medium. One of the main conclusions is that weak hydrophilic rock samples can obtain the highest E_d. Second, the relationship between pore structure and water E_d has been a subject that geologists and oil recovery engineers have been paying close attention (Gao et al., 1986; Okasha et al., 2005; Farzaneh et al., 2011; Huang et al., 2018). The pore structure of rock refers to the geometric shape, size, distribution and interconnection of pore and throat of rock. Some scholars start from the heterogeneity of pore structure by means of core mercury pressure data, then they think that there is a good linear relationship between them (Wang and Bao, 1999; Sun and He, 1999). However, many contradictions have been found in this research. For example, there is no close relationship between oil displacement efficiency and permeability, and there is even an inverse relationship between oil displacement efficiency and permeability. Due to the limitations of the study, there is no universally recognized rule (Zhong, 2000). The third aspect is the study on the influence of oil-water viscosity ratio on oil displacement efficiency. Some scholars pointed out that oil displacement efficiency has a significant negative correlation with the logarithm of oil-water viscosity ratio (Wensheng, 2003; Zhang et al., 1995). Another important aspect is to study the effect of injection PV number on oil displacement efficiency. It believed that the core oil displacement efficiency increased with the increase of the injection PV number (Wang et al, 2002). They pointed out that after the observation that the water content was up to 99.98%, the core oil displacement efficiency could still be improved by increasing the injection PV number.

In addition, the relevant empirical formula has become one of the commonly used methods to study oil displacement efficiency. Some scholars have made statistical analysis on the test results of laboratory water flooding and obtained the mathematical model to predict the oil displacement efficiency. The relationship between the ultimate oil displacement efficiency with oil water viscosity ratio and air permeability was obtained based on the core water displacement test in the oil fields of China, the United States and the Soviet Union (Fen, 2009). According to development data of Shuanghe oil field, the multivariate regression relational expression between oil displacement efficiency and permeability, oil water viscosity ratio and injection ratio was built (Huang et al., 1997).

Oil displacement efficiency is a significant index in water drive oilfield, and is usually obtained by water drive cores experiments. In recent years, pioneer works were conducted on oil displacement efficiency. According to the characteristics of water drive reservoir, the method of applying geological parameters and production history data to forecast the oil displacement efficiency based on water flooding curve was deliberately deduced (Xianke, 2005). The oil displacement efficiency calculated by oil-water relative permeability test is only the final oil displacement efficiency of oil field. For this reason, the statistical rule of oil displacement efficiency and effective rock permeability in Bohai oilfield by taking the oil and water relative permeability curves measured by 283 natural cores of Bohai oilfield as a sample were obtained (Gong et al., 2015). At the same time, the calculation formula of water displacement oil efficiency is deduced theoretically by using relative permeability curve, fractional flow equation and Welge equation. Above all, the research results are at the same temperature. In this case, increasing PV is an important way to improve the

oil displacement efficiency.

For hot water or steam displacement, there are two ways to improve oil displacement efficiency. One is to reduce viscosity of crude oil and the residual oil saturation by increasing the temperature of the injected fluid. The other is to increase the total amount of injected fluid to improve oil washing efficiency. There is one question now, that is, for a particular reservoir, how do technical people make decisions? At the same time, many analytical models of performance prediction of SF are used in steam flooding project evaluation. The value of oil saturation change of heating area before and after steam injection is an important parameter for the analytical models. Whether this value is correct or not directly determines the accuracy of the prediction. Regrettably, this parameter is difficult to obtain, and an empirical value is usually taken in previous studies, which reduces the accuracy of project prediction. So, another question is, how to predict the value of oil saturation before and after steam injection precisely?

Therefore, the present study is concerned with solving the above two problems about thermal flooding oil displacement efficiency. At the beginning, one dimensional core displacement experiment was carried for hot water and steam, respectively. Then, dozens of curves and correlations about E_d varied with injection *PV* number and injection temperatures were regressed, respectively. Based on this, the formula of E_d and *PV*, E_d and *T* for injection hot water and steam was established respectively, which makes up for the shortage of the finite test data points. Next, chart of the E_d between the *PV* and *T* was obtained. Besides, sensitivity analyses of injection rate and steam quality are discussed in this paper. Finally, the precise of the regression formula was verified by three steam flooding case of different heavy oil fields. The results indicated that, in order to get higher E_d, higher injection *PV* and temperature are beneficial. With the E_d chart, technicians can determine different schemes to improve oil displacement efficiency according to specific reservoir conditions. Besides, main production indexes such as oil recovery can be predicted quickly and precisely.

ONE-DIMENSIONAL CORE DISPLACEMENT EXPERIMENT

In this section, one dimensional core displacement experiment data of a typical well B14M in heavy oil field are applied to explain the statistical approach to investigate oil displacement efficiency. The core samples of the test were frozen core samples from well B16, and the samples were drilled, sealed, pumped, washed and dried in the laboratory according to the requirements of the experience research. The determinations of high temperature relative permeability and oil displacement efficiency are based on the oil industry standard SY/T.

6315-2006 (SY/T, 2006).

Test method

Mainly including the following procedures:

(1) Fill the natural cores of N oil field after wash oil to single tube model (porosity and permeability are close to actual reservoir.
(2) Determine saturated water pore volume, and saturation oil to establish irreducible water, simulated the original reservoir conditions.
(3) Then, according to the requirements of high temperature relative permeability and oil displacement efficiency measurement standards, the unsteady method with constant speed was used to inject steam and hot water until the oil was not released at the outlet.
(4) Record the water and oil production at the outlet of the model, calculate the oil displacement efficiency under different displacement conditions according to the calculation method of oil displacement efficiency, and draw the oil displacement efficiency curve.

Test equipment

The oil displacement efficiency equipment is mainly composed of thermostat box, single pipe core holder, injection system, temperature pressure measurement and control system and output liquid measurement system. The main equipment includes thermostat box, high-pressure advection pump, steam generator, single pipe model, temperature display and control instrument, pressure regulator and air water separator.

Test scheme design

A total of 7 displacement comparative tests were conducted. During the test, 7 parallel sample simulation core models were established, and part of the physical parameters of the simulated core were shown in Table 1.

Test result data

Under the condition of displacement speed 20 ml/h, four oil displacement efficiency tests of were conducted at injection temperature of 56, 100, 150 and 200°C, respectively. Through displacement tests, oil-water separation and data processing, oil displacement efficiency curves at different water injection temperatures were obtained, as shown in Table 2 and Figure 1a.

Figure 1 shows that, water injection temperature has a significant influence on the oil displacement efficiency. It also shows that there are two ways to improve the oil displacement efficiency for hot water displacement: one is to keep the total amount of hot water (the same PV number), and to improve the oil displacement efficiency by raising the temperature. The other is to keep the injected fluid at the same temperature (sometimes restricted by the heat injection equipment) and increase the efficiency by increasing the volume of the injected fluid. The changes of the two methods are different at different stages, so quantitative analysis is needed.

Correlations studies based on statistical analysis

Relationship between oil displacement efficiency and PV at the same temperature

Figure 2 shows that, under the same water injection temperature, the oil E_d increases with the increment of injection PV number. Especially in the early stage of water flooding, with the increase of water injection, the oil E_d increases rapidly. When the injection PV number is between 0.5 and 0.7, it reaches the inflection point of the curve. Statistical studies show that the displacement efficiency has a good linear correlation with the natural logarithm of injection PV number. Therefore, the statistical relations at different temperatures can be obtained as formula 1 to formula 4.

Table 1. Physical parameters of physical model of hot water and steam flooding test.

Parameter	Value for water flooding	Value for steam flooding
Model permeability, mD	6201~6541	6386~6467
Model porosity, %	39.8~40.7	40.2~40.8
Oil saturation, %	80.9~82.1	80.0~82.6
Saturated oil temperature, °C	56	56
Model length, cm	15	15
Model diameter, cm	2.54	2.54
Displacement speed, mL/h	20	30
Displacement medium,	Hot Water	Superheated steam

Annotation: The saturated oil temperature 56°C is the original reservoir temperature of N oil field.

Table 2. Data table of hot water and steam drive effect at different temperatures.

Hot water								Steam					
56°C		100°C		150°C		200°C		200°C		240°C		280°C	
PV	E_d %	PV	E_d %	PV	E_d %	PV	E_d %	PV	E_d %	PV	E_d %	PV	E_d %
0.000	0.00	0.000	0.00	0.000	0.00	0.000	0.00	0.000	0.00	0.000	0.00	0.000	0.00
0.059	7.92	0.116	14.11	0.117	15.83	0.042	5.14	0.049	6.10	0.115	13.89	0.097	12.10
0.209	18.48	0.381	29.03	0.278	25.83	0.141	16.60	0.163	20.33	0.213	25.79	0.213	26.60
0.373	25.52	0.977	40.32	0.537	34.17	0.271	29.25	0.327	30.08	0.607	45.63	0.535	49.60
0.634	29.92	1.639	45.97	0.974	43.75	0.598	46.64	0.817	45.53	1.262	58.73	1.019	62.10
1.059	33.44	2.599	50.00	1.460	48.75	1.219	54.15	1.471	51.63	1.918	63.49	1.665	66.50
1.876	36.96	3.262	52.42	2.430	53.75	1.742	57.71	2.778	57.30	2.902	66.67	2.632	69.80
3.183	40.56	4.255	55.24	3.239	56.67	2.526	61.26	4.412	62.20	4.869	68.65	4.568	71.80
5.797	43.56	5.911	58.06	4.534	59.58	4.160	64.82	6.373	65.40	6.836	70.63	6.503	73.80
-	-	7.566	59.68	5.828	61.25	5.794	65.90	8.987	67.80	8.803	72.62	8.439	75.40
-	-	-	-	8.094	62.92	8.245	66.30	-	-	-	-	-	-

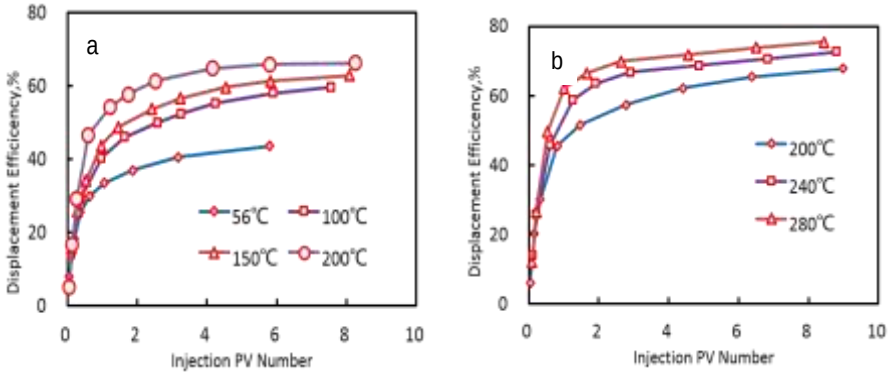

Figure 1. Comparison curve of oil displacement efficiency at different temperatures for (a) injection hot water, (b) injection steam.

$$E_{d-water56℃} = 7.8639\ln(PV) + 31.7428 \quad (R^2 = 0.9854) \tag{1}$$

$$E_{d-water100℃} = 10.9414\ln(PV) + 39.2214 \quad (R^2 = 0.9947) \tag{2}$$

$$E_{d-water150℃} = 11.5682\ln(PV) + 41.9314 \quad (R^2 = 0.9875) \tag{3}$$

$$E_{d-water200℃} = 12.5987\ln(PV) + 46.7483 \quad (R^2 = 0.9590) \tag{4}$$

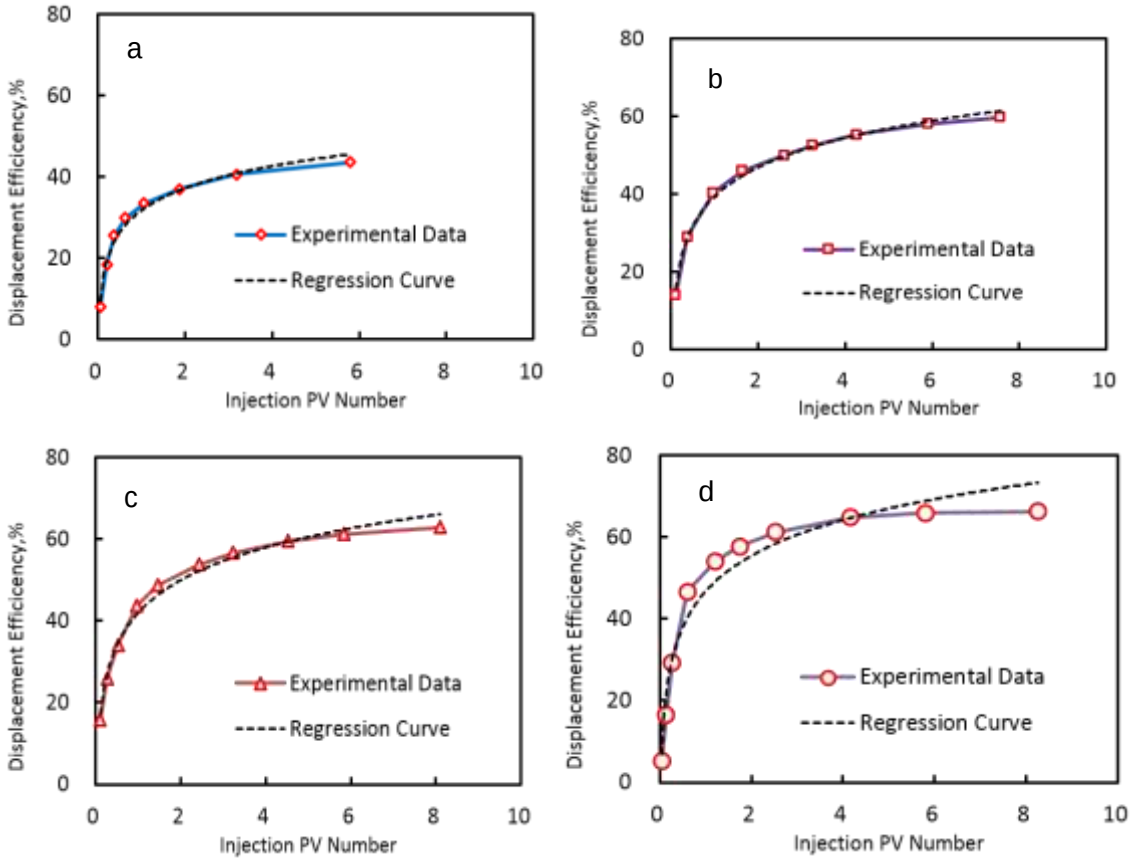

Figure 2. Comparison of oil displacement efficiency of experimental data and regression curve varied with temperature for (a) 56°C, (b)100°C, (c) 150°C, (d) 200°C.

The correlation coefficient R^2 is high, ranging from 0.9590 to 0.9947. By analyzing the above four equations, a rule can be obtained: at any temperature, a similar relation can be obtained, which can be expressed as Equation 5.

$$E_{d-water} = a\ln(PV) + b \quad (5)$$

Since the number of tests is limited, displacement efficiency beyond the test temperature range cannot be obtained, and the relationship between oil displacement efficiency and PV number at any temperature can be calculated by equation 5. Where, *a* and *b* are slope and intercept of linear relation respectively. In order to get corresponding relation between temperature and the oil displacement efficiency, the corresponding relations between coefficient a, b and injection temperature were established respectively, which were shown in Figure 3, formula 6, formula 7.

$$a = 3.6009\ln T - 6.3069 \quad (R^2 = 0.9514) \quad (6)$$

$$b = 11.2658\ln T - 13.4311 \quad (R^2 = 0.9827) \quad (7)$$

Substitute formula 6 and formula 7 into formula 5, oil displacement efficiency is obtained and the relation between the water injection PV and injection temperature can be expressed by formula 8.

$$E_{d-water} = 3.6009\ln T\ln(PV) - 6.3069\ln(PV) + 11.2658\ln T - 13.4311 \quad (8)$$

Relationship between oil displacement efficiency and temperature at the same PV

The oil displacement efficiency of different injection temperatures at the same PV number can be plotted in Figure 4. Figure 4 shows that the oil displacement efficiency is increased with water injection temperature increment at different injection PV number. Statistical studies show that the displacement efficiency has a good linear correlation with the injection temperature at different PV number. Therefore, the statistical relations of E_d and T at different PV number can be obtained as Equations 9 to14.

$$E_{d-water\ 0.5\ PV} = 0.0773T + 22.6826 \quad (R^2 = 0.9698) \quad (9)$$

$$E_{d-water\ 1.0\ PV} = 0.0984T + 27.4629 \quad (R^2 = 0.9540) \quad (10)$$

$$E_{d-water\ 1.5\ PV} = 0.1107T + 30.2592 \quad (R^2 = 0.9462) \quad (11)$$

$$E_{d-water\ 2.0\ PV} = 0.1195T + 32.2433 \quad (R^2 = 0.9414) \quad (12)$$

$$E_{d-water\ 2.5\ PV} = 0.1263T + 33.7822 \quad (R^2 = 0.9379) \quad (13)$$

$$E_{d-water\ 3.0PV} = 0.1318T + 35.0396 \quad (R^2 = 0.9353) \quad (14)$$

The correlation coefficient R^2 is high, ranging from 0.9353 to 0.9698. By analyzing the above six formulas, a rule can be obtained:

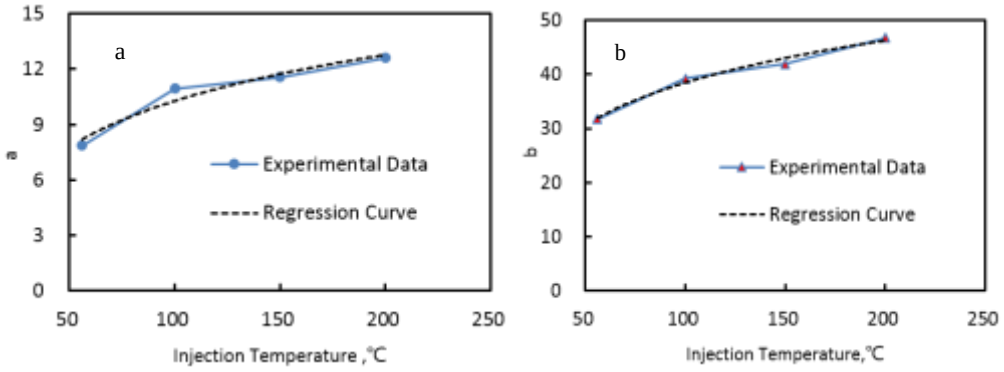

Figure 3. Diagram of the relationship between the injected fluid temperature and the coefficient (a) slope a, (b) intercept b.

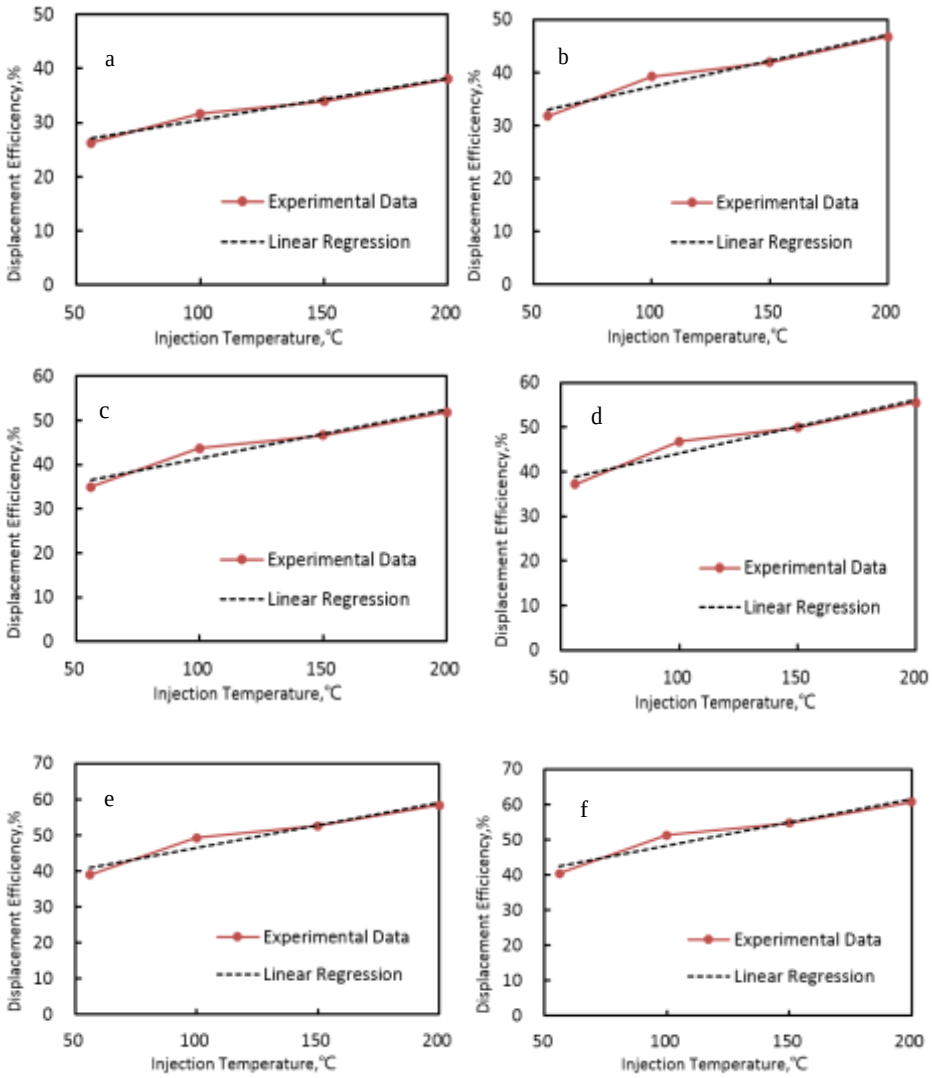

Figure 4. Comparison of oil displacement efficiency of hot water experimental data and regression curve varied with injection PV number for (a) 0.5 (b)1.0 (c)1.5 (d)2.0 (e) 2.5 (f)3.0.

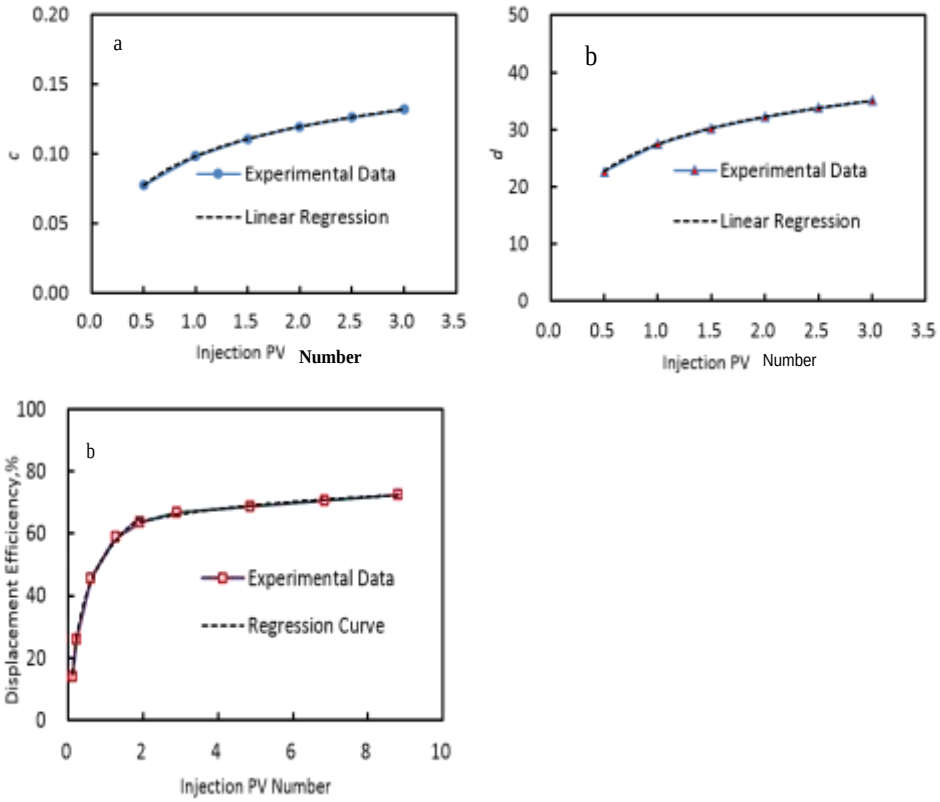

Figure 5. Diagram of the relationship between the injected PV number and the coefficient (a) slope c, (b) intercept d.

at any temperature, a similar relation can be obtained, which can be expressed as Equation 15.

$$E_{d-water} = cT + d \quad (15)$$

In order to get corresponding relation between injection PV number and the oil displacement efficiency, the corresponding relation between coefficient of c, d and injection PV number were established respectively, which are shown in Figure 5, formula 16, formula 17.

$$c = 0.0304\ln(PV) + 0.0984 \quad (R^2 = 1.0) \quad (16)$$

$$d = 6.8966\ln(PV) + 27.4629 (R^2 = 1.0) \quad (17)$$

Substitute formula 16 and formula 17 into formula 15, oil displacement efficiency is obtained. Moreover, formula 18 can express the relation between the water injection PV and injection temperature.

$$E_{d-water} = 0.0304T\ln(PV) + 0.0984T + 6.8966\ln(PV) + 27.4629 \quad (18)$$

Changing injection medium from hot water to steam

Water can exist in different states at different temperatures and pressures. Compared with hot water, steam has the characteristics of higher heat carrying capacity and greater specific capacity, etc., which is very beneficial to improve the thermal recovery effect. Therefore, steam is a common medium for thermal oil production (Hou and Sun, 2013). Under the injection speed of 30 ml/h (water equivalent) conditions, steam flooding experiments at different steam injection temperature for 200, 240 and 280°C were carried out, result were shown in Table 2 and Figure 1(b). With the increase of steam injection temperature, oil displacement efficiency also increases, but the amplitude of increase is small. Only 9.1% oil displacement efficiency was increased by raising the temperature from 200 to 280°C.

The experimental data showed different change ranges under different PV numbers, so it was necessary to carry out regression by subdivided into two segments of 0<PV<2 and PV>2. Therefore, the statistical relations at different temperatures can be obtained as Equations 19 to 21 which are shown in Figure 6.

$$\begin{cases} E_{d-steam\,200^\circ C} = 13.7822\ln(PV) + 46.6218 & (R^2 = 0.9949) \quad (0 < PV < 2) \\ E_{d-steam\,200^\circ C} = 9.12711\ln(PV) + 48.1979 & (R^2 = 0.9968) \quad (2 < PV < 10) \end{cases} \quad (19)$$

$$\begin{cases} E_{d-steam\,240^\circ C} = 17.9543\ln(PV) + 53.4439 & (R^2 = 0.9968) \quad (0 < PV < 2) \\ E_{d-steam\,240^\circ C} = 5.64061\ln(PV) + 60.0674 & (R^2 = 0.9861) \quad (2 < PV < 10) \end{cases} \quad (20)$$

$$\begin{cases} E_{d-steam\,280^\circ C} = 20.1312\ln(PV) + 59.3897 & (R^2 = 0.9881) \quad (0 < PV < 2) \\ E_{d-steam\,280^\circ C} = 5.22701\ln(PV) + 64.1403 & (R^2 = 0.9884) \quad (2 < PV < 10) \end{cases} \quad (21)$$

The correlation coefficient R^2 is high, ranging from 0.9881 to 0.9968.By analyzing the above formulas, a rule can be obtained which can be expressed as Formula 22.

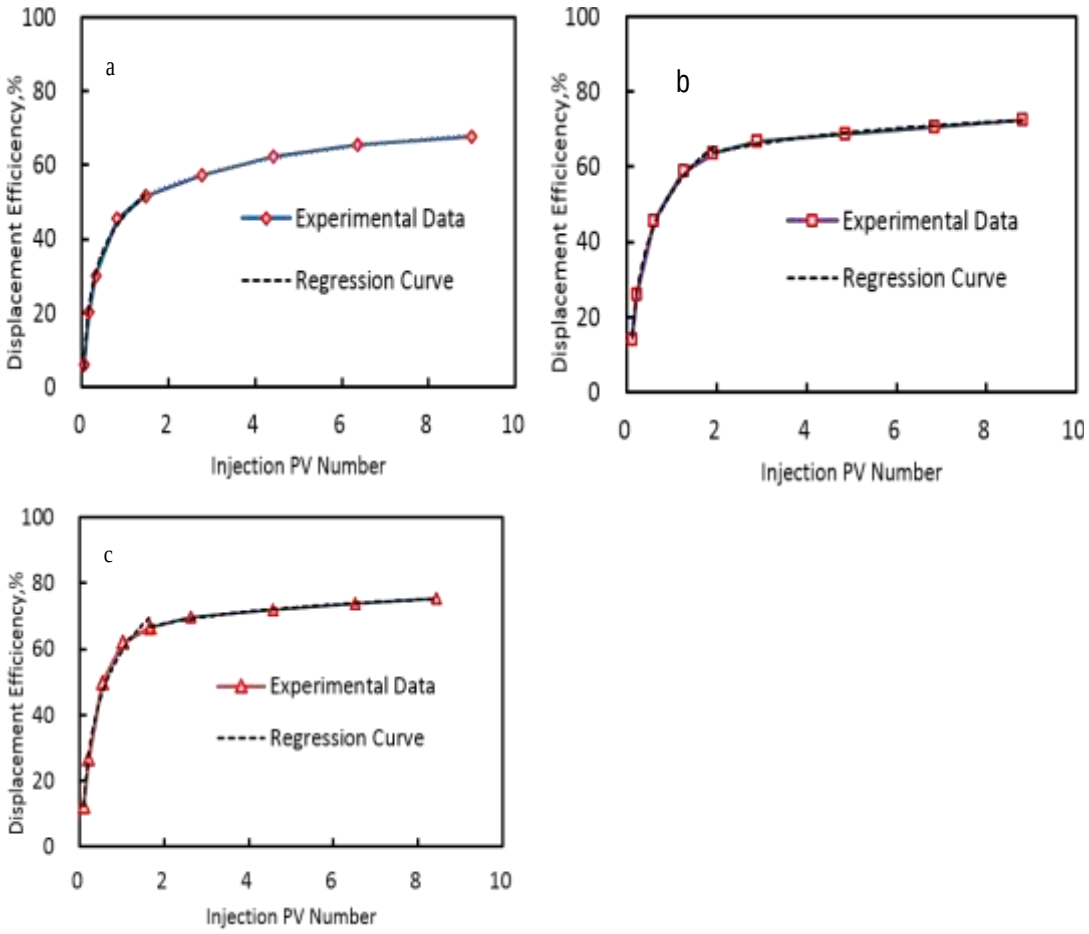

Figure 6. Comparison of oil displacement efficiency of steam flooding experimental data and regression curve varied with temperature for (a) 200°C, (b) 240°C (c) 280°C.

$$\begin{cases} E_{d-steam} = \mathbf{e}\ln(PV) + \mathbf{f} & (0 < PV < 2) \\ E_{d-steam} = \mathbf{g}\ln(PV) + \mathbf{h} & (2 < PV < 10) \end{cases} \quad (13)$$

The corresponding relations between coefficient e, f, g , h and injection temperature are established respectively, which were shown in Figure 7, formula 23, formula 24, formula 25, formula 26.

$$e = 18.9904\ln T - 86.6121 \quad (R^2 = 0.9829) \quad (23)$$

$$f = 37.9304\ln T - 154.3750 \quad (R^2 = 0.9999) \quad (24)$$

$$g = 34.3725e^{-0.0070T} \quad (R^2 = 0.8503) \quad (25)$$

$$h = 47.9157\ln T - 204.6904 \quad (R^2 = 0.9494) \quad (26)$$

Substitute formula 23 to formula 26 into formula 22, oil displacement efficiency is obtained and the relation between the water injection PV and injection temperature can be expressed by formula 27.

$$\begin{cases} E_{d-steam} = 18.9904\ln T\ln(PV) - 86.6121\ln(PV) + 37.9304\ln T - 154.3750 & (0 < PV \\ E_{d-steam} = 34.3725e^{-0.0070T}\ln(PV) + 47.9157\ln T - 204.6904 & (2 < PV < \end{cases} \quad (27)$$

Average oil saturation prediction model

When the oil saturation of the pore volume affected by water drops to the remaining oil saturation, the displacement efficiency is expressed as follows (Jiang et al., 2006):

$$E_d = 1 - \frac{S_{or}}{S_{oi}} \cdot \frac{B_{oi}}{B_o} \quad (28)$$

If the oil volume is constant, the above equation can be rewritten as:

$$E_d = 1 - \frac{S_{or}}{S_{oi}} \quad (29)$$

The oil displacement efficiency calculated by formula 29 is the extreme oil displacement efficiency. The displacement at a certain time of water injection can be calculated by the following formula:

$$E_d = \frac{\bar{S}_{oi} - \bar{S}_o}{\bar{S}_{oi}} \quad (28)$$

Substitute formula 30 into formula 18, it can be got that:

$$\frac{\bar{S}_{oi} - \bar{S}_o}{\bar{S}_{oi}} = 0.0304T\ln(PV) + 0.0984T + 6.8966\ln(PV) + 27.4629 \quad (29)$$

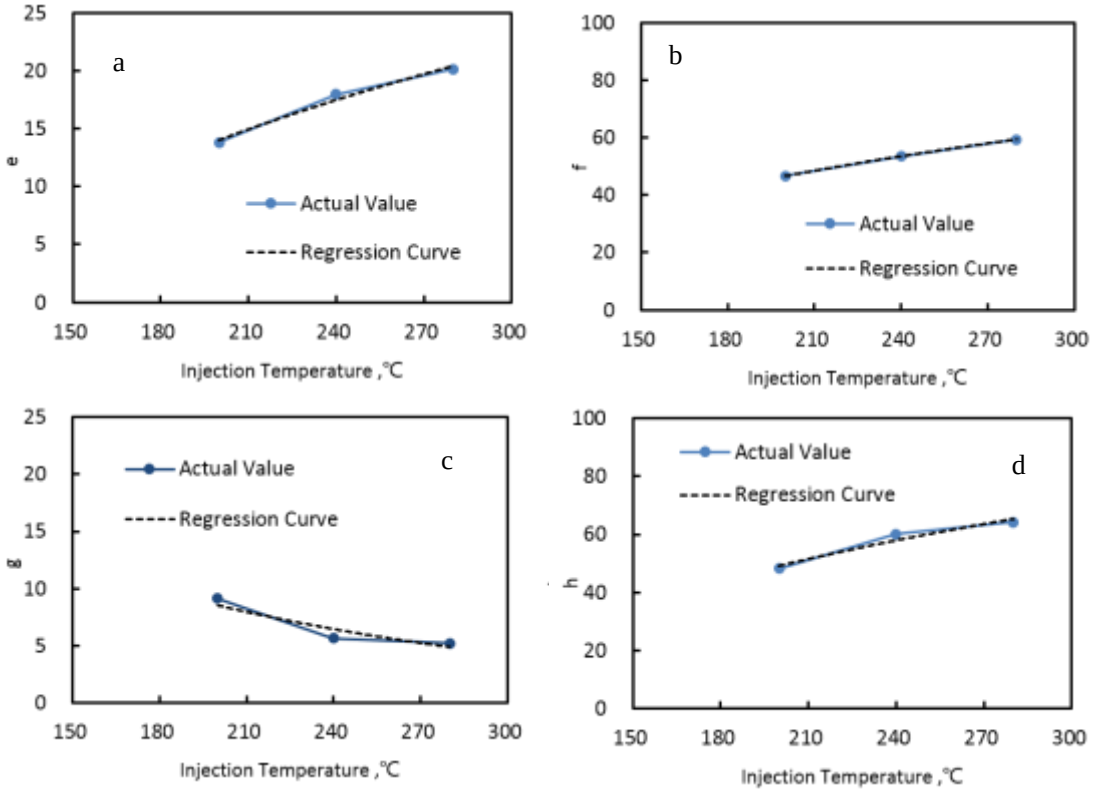

Figure 7. Diagram of the relationship between the injected temperature and the coefficient (a) slope e, (b) intercept f, (c) slope g, (d) intercept h.

Substitute formula 30 into formula 27, it can be got that:

$$\begin{cases} \frac{\bar{s}_w-\bar{s}_{wi}}{\bar{s}_{oi}} = 18.9904\ln T\ln(PV) - 86.6121\ln(PV) + 37.9304\ln T - 154.3750 \quad (0 < PV < 2 \\ \frac{\bar{s}_w-\bar{s}_{wi}}{\bar{s}_{oi}} = 34.3725e^{-0.0070T}\ln(PV) + 47.9157\ln T - 204.6904 \quad (2 < PV < 10 \end{cases} \tag{30}$$

For injection hot water and steam, Formula (31) and (32) can estimate the current oil saturation at different PV numbers and temperatures, respectively.

RESULTS AND DISCUSSION

Oil displacement efficiency chart and its application

According to formula 18 and formula 27, the correlation between injection temperature and PV number can be obtained under different oil displacement efficiency conditions, which has been shown in Figure 8.

The four curves of Figure 8 (a), each curve indicates different oil displacement efficiency. Moreover, four curves are 30, 40, 50 and 60% from left to right, respectively. The abscissa represents in injection pore volume ratio, ordinate represents the corresponding injection temperature. For any one of these curves, the injection PV number is negatively correlated with the injection temperature. In other words, the same oil displacement efficiency, the higher the temperature, the lower the PV injected. The lower the temperature, the greater the PV injected. For steam injection, it has the same characteristics, as shown in Figure 8 (b).

Sensitivity analysis of injection rate and steam quality

The first parameter is the injection rate of water. At water injection temperature of 100°C, four speeds of 57, 100, 200, 100 m^3 /d were investigated. The corresponding water injection speed is reduced to 20, 35, 70, 105 mL/h respectively for single tube model. Figure 9 shows the effect of different injection rates on slope *a* and intercept *b*. The quantitative expressions are shown in formula 33 and formula 34.

$$a = 11.8789e^{-0.0019V} \ (R^2 = 0.9783) \tag{33}$$

$$b = 5.4188\ln V + 17.2302 \ (R^2 = 0.9186) \tag{34}$$

The second parameter is the steam injection speed.

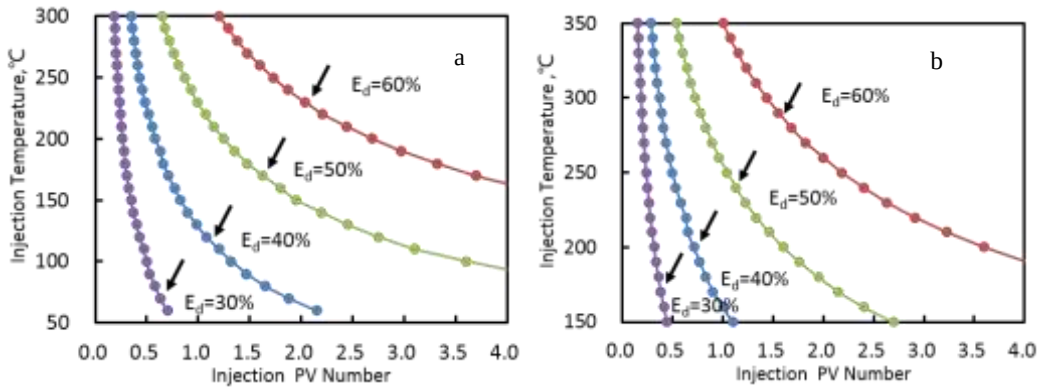

Figure 8. Diagram of the relationship between the injected temperature and the injection PV number of (a) hot water, (b) steam.

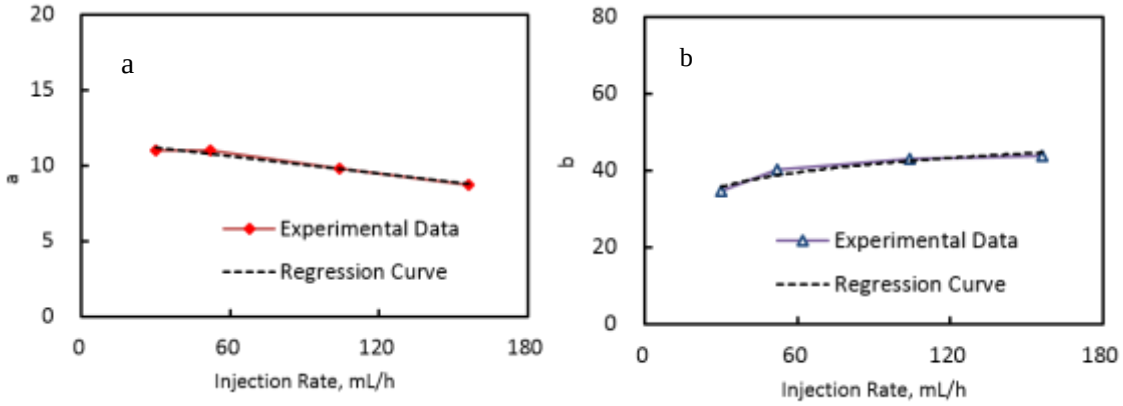

Figure 9. Diagram of the relationship between the injected rate and the coefficient (a) slope a, (b) intercept b.

Under the injection temperature of 240°C condition, four speeds of 45, 80, 160, and 80 m^3/d were carried out. And in laboratory, the corresponding injection rates of one dimension core are 30, 52, 104, 156 mL/h respectively. Figure 10 shows the effect of different injection rates on slope e and g and intercept f and h. The quantitative expressions are shown in formula 35 to formula 38.

$$e = -0.0444V + 18.7167\ (R^2 = 0.9593) \quad (35)$$

$$f = 62.7803e^{-0.0024V}\ (R^2 = 0.9640) \quad (36)$$

$$g = 1.9120\ln V - 0.3769\ (R^2 = 0.8741) \quad (37)$$

$$h = 55.4786e^{-0.0023V}\ (R^2 = 0.9504) \quad (38)$$

The third parameter is the steam quality, that is, the mass percentage of dry saturated steam containing in per kilogram of wet steam. Under the condition of steam injection temperature 240°C and steam injection rate of 52 ml/h, four different steam quality tests of 20, 40, 50, 70% were carried out, respectively. Figure 11 shows the effect of different injection rates on slope e and g and intercept f and h. It can be concluded that the steam quality has little effect on the slope e and g, intercept f and h. Therefore, in steam flooding progress, the steam quality mainly increases the swept volume, not the oil displacement efficiency.

Calculate the change value of oil saturation in heated zone

In many analytical models of dynamic prediction of thermal recovery, there is a parameter ΔS_o, that is, the oil saturation change value of reservoir before and after steam displacing (Myhill and Stegemeier, 1978; Butler and Stephens, 1981; Chandra and Mamora, 2005; Huang et al., 2016). It is a core and indispensable parameter of the analytical model, such as steam drive and steam

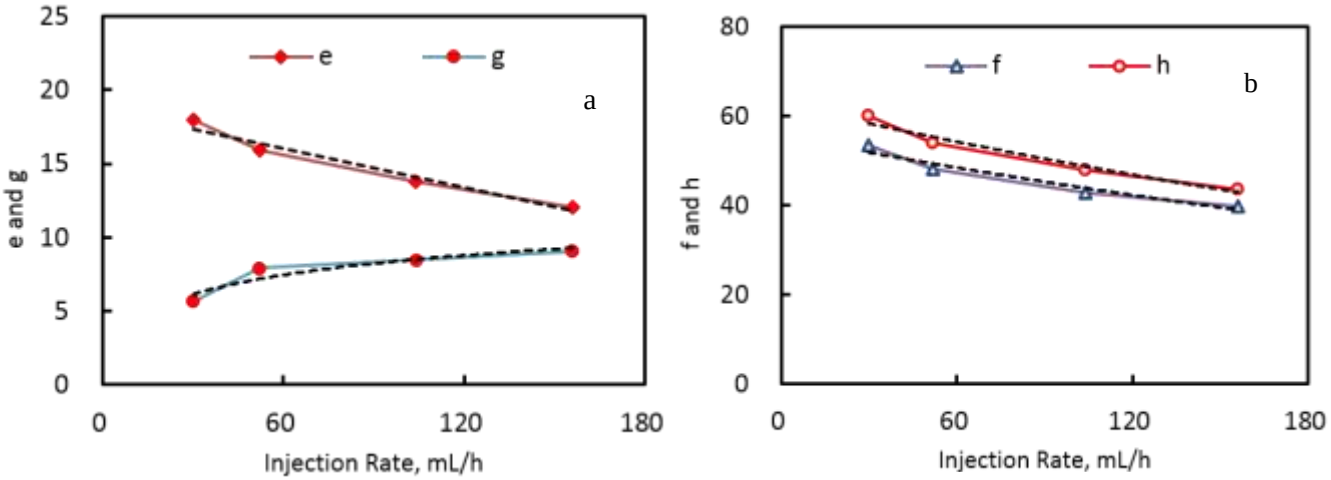

Figure 10. Diagram of the relationship between the injected rate and the coefficient (a) slope e and g, (b) intercept f and h. Real line: experimental data. Dotted line: regression curve.

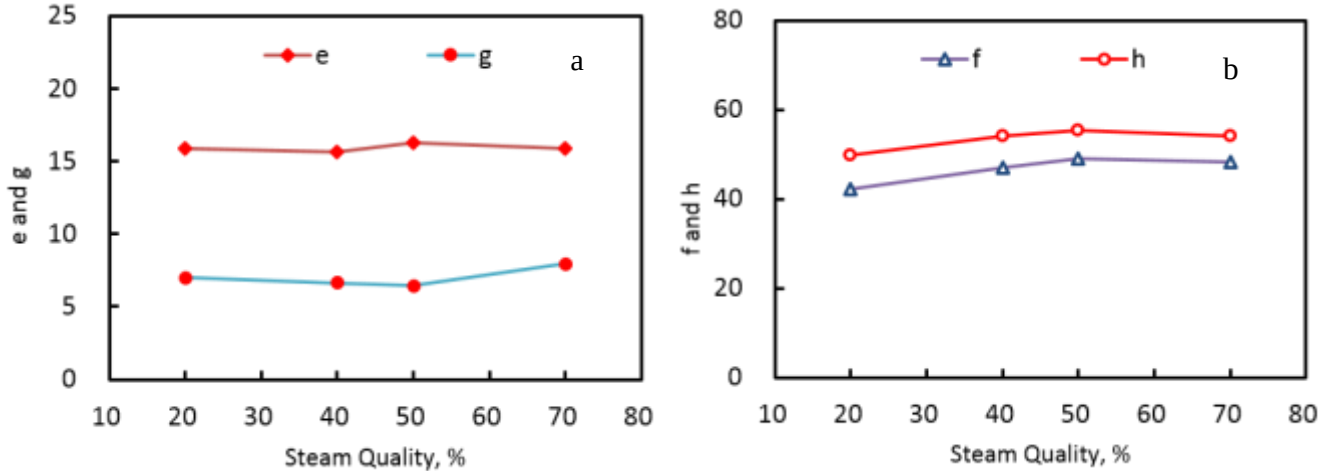

Figure 11. Diagram of the relationship between the injected rate and the coefficient (a) slope e and g, (b) intercept f and h.

Assisted gravity oil discharge. So accurate predicting the value of ΔS_o is of great importance for predicting thermal dynamic. According to formula 30 and formula 31, the oil saturation in different injection temperatures and PV numbers can be obtained for a steam-flooding oilfield.

To verify the accuracy of the calculation model, using the product of the sweep efficiency (E_v) and displacement efficiency (E_d) as the ultimate recovery method, three steam flooding project of different heavy oil fields of literature 6 were taken as a calculation case. The three oil fields contain Schoonebeek-in the eastern part of Netherlands, San Ardo in Monterey County, California, USA and Hamaca in Venezuela's Orinoco heavy oil belt. Basic parameters of the three fields were shown in Table 3, and the ultimate recovery calculation results were shown in Table 4. By contrasting the results of the three analytical model presented in the literature (Ankit and Ajay, 2012) and the actual result, it can be seen that , this paper calculation forecasts maximum recovery is very close to the oil field actual situation. Therefore, the model in this paper provides guidance for steam flooding evaluation in the early stages of the project.

The advantages and limitations of the model

The regression relational expressions are more convenient to calculate the oil displacement efficiency under the different injection temperatures and injection PV numbers. Moreover, this can be helpful for steam

Table 3. Reservoir characteristic and operating conditions of Schoonebeek, San Ardo and Hamaca fields (Refer to reference [6] for details) [6].

Parameter	Schoonebeek	San Ardo	Hamaca fields
Permeability, mD	1000-10000	6922	12000
Porosity, %	30	34.5	30
Initial oil saturation, %	47	73	83.2
Residual oil saturation, %	25	15	15
Reservoir temperature, °C	37.8	52.8	51.7
Initial oil viscosity under reservoir temperature, cp	180	3000	25000
Net thickness, m	25.3	35.1	30.5
Injection rate, cold water equivalent ,m^3/day	198.7	254.4	254.4
Steam quality, fraction	0.7	0.8	0.8
Total day of calculations, days	2190	6900	6900
Injection PV number	0.60	1.71	1.70
Injection temperature **(°C)**	176.7	305.7	305.7
Average oil saturation after steam flooding predicted by Formula (31), fraction	0.289	0.247	0.282
Displacement efficiency predicted by Formula (30), fraction	0.386	0.661	0.661
Average swept volume efficiency by reference 6 (%)	70.5	34.0	36.6
Maximum recovery forecasts by this article	27.20	22.50	24.20

Table 4. Comparison of maximum recovery as predicted by different models.

Oil recovery (fraction)	Schoonebeek field (%)	San Ardo field (%)	Hamaca field (%)
Jeff Jones model	18.00	22.89	16.00
Suandy Chandra model	46.00	43.00	40.00
Actual field value	33.00	27.00	30.00
Forecasts by this article	27.20	22.50	24.20

flooding performance prediction, and provides a precise oil saturation change value for analytical model, which can improve the accuracy of forecasting model.

Therefore, the main meaning and purpose of this research is to provide guidance for the evaluation steam-flooding project of heavy oil.

Although a lot of important relations and results have been achieved, there are still some shortcomings that need to be further improved later. The oil displacement efficiency obtained from core test mainly depends on geological factors and fluid properties, such as reservoir type, pore- structure, reservoir heterogeneity, rock wettability and crude oil viscosity. The oil displacement efficiency is a macroscopic oil displacement efficiency of oil field level and scale. The final recovery is the product of displacement efficiency and sweep volume coefficient. A major problem, therefore, is the microscopic oil displacement efficiency obtained by core test, represents the coring with special pore structure of itself. Therefore, it can achieve more satisfactory results only to those with the similar permeability, porosity, etc. Therefore, in order to improve the study, the number of statistical samples can be increased and make the coefficient value of more general significance.

Conclusion

Precise description the displacement efficiency is extremely important for evaluating the performance, economic effectiveness and final recovery. Current researches mainly focused on one-dimensional core displacement experiment. Regretfully, each experiment has a finite number of data points, and it is difficult to obtain data and laws beyond range of test points. In this study, the effect of injection PV number and injection temperature on oil displacement efficiency was analyzed and evaluated quantitatively. Several valuable conclusions can be drawn from the previously mentioned research.

For hot water or steam displacement, the oil displacement efficiency is not only affected by injection PV number but also the injection temperature. Based on one-dimensional core displacement experiment, dozens of curves and correlations about displacement efficiency varied with injection PV number, injection temperature

were regressed, respectively.

Based on dozens of curves, the formula of displacement efficiency of injection hot water and injection steam was established respectively. It makes up for the shortage of the finite test data points.

Chart of the displacement efficiency between the injection PV number and injection temperature was obtained. It is helpful for steam flooding performance prediction.

The precise of the regression formula was verified by three steam flooding case of different heavy oil fields. Main production indexes of heavy oil field such as oil recovery can be predicted quickly and precisely.

ACKNOWLEDGEMENT

The authors wish to thank the Tianjin Branch of CNOOC Ltd., China National Offshore Oil Corporation. This work was supported by the National Science and Technology Major of China (2016ZX05058-001-008), which was named optimization and application of thermal recovery in offshore heavy oil fields.

CONFLICT OF INTERESTS

The authors have not declared any conflict of interest.

Nomenclature

$E_{d-water\,56℃}$, % Oil displacement efficiency for Injection 56℃ water; $E_{d-water\,100℃}$, % Oil displacement efficiency for Injection 100℃ water; $E_{d-water\,150℃}$, % Oil displacement efficiency for Injection 150℃ water; $E_{d-water\,200℃}$, % Oil displacement efficiency for Injection 200℃ water; $E_{d-water}$, % Oil displacement efficiency for Injection water; PV, Decima Pore volume multiple; $\mathbf{a}$ Slope of linear relation; $\mathbf{b}$ Intercept of linear relation; T, ℃ Temperature; $\mathbf{e}$ Slope of linear relation; $\mathbf{f}$ Intercept of linear relation; $\mathbf{g}$ Slope of linear relation; $\mathbf{h}$ Intercept of linear relation; $E_{d-steam\,200℃}$,% Oil displacement efficiency for Injection 200℃ steam; B_{oi} Volume coefficient of crude oil before water injection; B_o Volume coefficient of crude oil after water injection; $\overline{S}_{oi}$, Decima Average oil saturation in water injection; $\overline{S}_o$, Decima Average oil saturation after water injection; S_{or}, Decima Residual oil saturation after water injection; $\mathbf{v}$, ml/h Injection rate of hot water or steam.

REFERENCES

Alboudwarei (2006). Highlighting heavy oil. Oilfield Review 18:34-53.

Anderson WG (1987). Wettability Literature Survey - Part 6: The Effect of Wettability on Waterflooding. Wettability Literature Survey–Part 6:1605-1622

Morrow NR (1990). Wettability and Its Effect on Oil Recovery. Journal of Petroleum Technology 42(12):1-476.

Ankit D, Ajay M (2012). Modified analytical model for prediction of steam flood performance. Journal of Petroleum Exploration and Production Technology 2:117-123.

Bao Y, Wang JY, Ian D. Gates (2016). On the physics of cyclic steam stimulation. Energy 115(1):969-985.

Butler RM (1991). Thermal recovery of oil and bitumen. New Jersey: Prentice Hall.

Butler RM, Stephens DJ (1981). The gravity drainage of steam-heated heavy oil to parallel horizontal wells. Journal of Canadian Petroleum Technology 20(2):36.

Chandra S, Mamora DD (2005) Improved steam flood analytical model. In: Paper (SPE 97870), SPE-PE/CIM-CHAO International Thermal operations and heavy oil symposium, Calgary, 1–3 Nov.

Donaldson EC, Thomas RD (1971). Microscopic Observations of Oil Displacement in Water Wet and Oil Wet Systems. SPE3555. Society of Petroleum Engineers (https://www.onepetro.org/conference-paper/SPE-3555-MS).

Dong L, Li Y, Zhang F (2012). Reservoir applicability of steam stimulation supplemented by flue gas. China Offshore Oil and Gas 24(S1):62-66.

Dong X, Liu H, Pang Z, Wang C, Lu C (2014a). Flow and heat transfer characteristics of multi-thermal fluid in a dual-string horizontal well. Numerical Heat Transfer, Part A: Applications 66:185-204.

Dong XH, Liu HQ, Hou JR, Chen ZX (2016). Transient fluid flow and heat transfer characteristics during co-injection of steam and condensable gases in horizontal wells. Journal of China University of Petroleum Education and Natural Science 40(2):105-114.

Dong XH, Liu HQ, Zhang ZX (2014b). The flow and heat transfer characteristics of multi-thermal fluid in horizontal wellbore coupled with flow in heavy oil reservoirs. Journal of Petroleum Science Engineering 122:56-68.

Escobar E, Valko P, Lee WJ, Rodriguez MG (2000). Optimization methodology for yclic steam injection with horizontal wells. In: Proceedings of the SPE 65525, paper presented at SPE/CIM international conference on horizontal well technology held in Calgary, Alberta, Canada; 6–8 November.

Farzaneh SA, Dehghan AA, Kharrat R, Ghazanfari MH (2011). An Experimental Investigation of Fracture Physical Properties on Heavy Oil Displacement Efficiency during Solvent Flooding. Energy Sources Part A-recovery Utilization and Environmental Effects 33(21):1993-2004.

Fen L (2009). Study on Water Displacement Efficiency and Sweep Efficiency for Sandstone Reservoir with Medium or High Permeability. Shandong, China University of Petroleum (East China), pp. 1-60.

Gao Y, Shen P, Tu F (1986). A study of pore structure by image processing method and its application. In International Meeting on Petroleum Engineering. Society of Petroleum Engineers. https://www.onepetro.org/conference-paper/SPE-14872-MS

Gong L, Yang X, Geng N (2015). The Study on Oil-water Relative Permeability and Displacement Efficiency in Bohai Oilfield. Journal of Yangtze University (Natural Science Edition) 12(4):61-65.

Hou J, Chen YM (1997). An improved steam soak predictive model. Petroleum Exploration Development 24(3):53-56.

Hou J, Sun J (2013). Thermal oil recovery technology. Shandong, China University of Petroleum (East China), Press pp. 38-44.

Hou J, Wei S, Du QJ, Wang JC, Wang QL, Zhang GF (2016c). Production prediction of cyclic multi-thermal fluid stimulation in a horizontal well. Journal of Petroleum Science Engineering 146:949-958.

Hou J, Xia ZZ, Li SX, Zhou K, Lu N (2016b). Operation parameter

optimization of a gas hydrate reservoir developed by cyclic hot water stimulation with a separated zone horizontal well based on particle swarm algorithm. Energy 96(1):581-591.
Hou J, Zhou K, Zhao H, Kang XD, Wang ST, Zhang XS (2016a). Hybrid optimization technique for cyclic steam stimulation by horizontal wells in heavy oil reservoir. Computer and Chemical Engineering 84(4):363-370.
Huang S, Cao M, Cheng L (2018). Experimental study on the mechanism of enhanced oil recovery by multi-thermal fluid in offshore heavy oil. International Journal of Heat and Mass Transfer 122(2018):1074-1084.
Huang Shijun, Xiong Hao, Wei Shaolei (2016). Physical simulation of the interlayer effect on SAGD production in mackay river oil sands. Fuel 183:373-385.
Huang Xuebin, Lu Guofu, Zhang Renxiong (1997). A Method for Prediction of Oil Displacement Efficiency in Water Drive Sandstone Reservoir. Henan Petroleum 11(4):15-16.
Jiang H, Yao J, Jiang R (2006). Principles and methods of reservoir engineering [M]. Shandong, China University of Petroleum Press, pp. 105-107.
Khansari Z, Kapadia P, Mahinpey N, Gates ID (2014). A new reaction model for low temperature oxidation of heavy oil: experiments and numerical modeling. Energy 64:419-428.
Liu D, Huang Y, Pan G (2018). Research on Multiple Thermal Fluid Stimulation for Offshore Heavy Oil Production. Special Oil and Gas Reservoirs 22(4):118-120.
Mahood HB, Campbell AN, Sharif AO, Thorpe RB (2016). Heat transfer measurement in a three-phase direct-contact condenser under flooding conditions. Applied Thermal Engineering 95:106-114.
Munawar K, Robert LL, Ning L (2015). Hematite nanoparticles in aquathermolysis: A desulfurization study of thiophene. Fuel 145:214-220.
Myhill NA, Stegemeier GL (1978). Steam-drive correlation and prediction. Journal of Petroleum Technology 30:173-182.
Okasha TM, Funk JJ, Al-Shiwaish AJA (2005). Evaluation of Residual Oil Saturation and Recovery Efficiency of Two Distinct Arabian Carbonate Reservoirs. In SPE Middle East Oil and Gas Show and Conference. Society of Petroleum Engineers.
Sheikholeslami M, Hayat T, Alsaedi A, Abelman S (2016). Numerical analysis of EHD nanofluid force convective heat transfer considering electric field dependent viscosity. International Journal of Heat and Mass Transfer 108:2558-2565.
Sun Wei, He Juan (1999). Displacing efficiency and affecting factors of reservoirs in Yan'an formation, Jiyuan Region Journal of Oil and Gas Geology 20(1):26-29.
SY/T 6315 (2006). Relative permeability and displacement efficiency test under the condition of high temperature for heavy oil reservoir. China's industry standard.
Wang C, Liu H, Wang J, Wu Z, Wang L (2016). Three-dimensional physical simulation experiment study on carbon dioxide and dissolver assisted horizontal well steam stimulation in super heavy oil reservoirs. Journal of Petroleum Exploration and Production Technology 6(4):825-834.
Wang D, Muchang G, Gang W (2002). The Influence of Multi-pore Volume Water Flooding on Pore Structure and Recovery of Lacustrine Deposit Mixed Wettability Cores. SPE77873. In SPE Asia Pacific Oil and Gas Conference and Exhibition. Society of Petroleum Engineers. https://www.onepetro.org/conference-paper/SPE-77873-MS
Wang Y, Bao Y (1999). Relationship Between Reservoir Pore Structure and Displacement Efficiency. Henan Petroleum 1:23-25.
Wensheng L (2003). A study on displacement characteristics of SZ36-1 oilfield. China Offshore Oil and Gas (Geology) 17(3):181-184.
Xiong H, Huang S, Liu H (2017). A Novel Optimization of SAGD to Enhance Oil Recovery-The Effects of Pressure Difference. IOR NORWAY 2017–19th European Symposium on Improved Oil Recovery, Stavanger, Norway, 24-27 April.
Xiong H, Huang S, Liu H, Cheng L, Li J, Xiao P (2017). A Novel model to investigate the effects of injector-producer pressure difference on SAGD for bitumen recovery. International Journal of Oil, Gas and Coal Technology 16(3):217-235.
Xu A, Mu L, Fan Z, Wu X, Zhao L, Bo B, Xu T (2013). Mechanism of heavy oil recovery by cyclic superheated steam stimulation. Journal of Petroleum Science and Engineering 111:197-207.
Yang Y, Huang SJ, Yang L, Song QL, Wei SL, Xiong H (2016). A multistage theoretical model to characterize the liquid level during steam-assisted-gravity-drainage process. Society of Petroleum Engineers Journal 1–12. June. 22(01):327-338.
Zhang R, Gao Y, Li J (1995). Effect of displacement conditions on water displacement efficiency of breccia reservoir. Henan Petroleum 9(4):32-37.
Zhao David W, Wang Jacky, Gates Ian D (2013). Optimized solvent-aided steam flooding strategy for recovery of thin heavy oil reservoirs. Fuel 112:50-59.
Zhong C (2000). The study on the relationship between pore structure and displacement efficiency. Petroleum Exploration and Development 27(6):45-46.

Related Journals: